University of Nottingham
UK | CHINA | MALAYSIA

Towards Organophosphonate-Functionalised Polyoxotungstate-Based Metal–Organic Frameworks

Chih-Huan Shen

20212835

Supervised by

Dr Graham Newton

Thesis submitted for the degree of Master of Research

School of Chemistry

The University of Nottingham

Acknowledgements

I would like to express my gratitude to Dr. Graham Newton, my Master of Research supervisor and mentor. His knowledge and guidance have been invaluable throughout my academic year, greatly expanding my understanding in research area. I am especially thankful for his kindness and passion, which have encouraged and inspired me, making this experience truly meaningful.

I am also very grateful to Dr. Kieran Jones for guiding me to think more deeply and investigate questions thoroughly, and for his patient and passionate discussions. I have benefited greatly from his approach to research.

My sincere thanks also go to Dr. Jack Jordan for his support in training me in laboratory techniques and helping me adjust to a new environment. I deeply appreciate his willingness to answer any question, no matter how small.

I would also like to thank everyone in the NAMI group for their help in the lab, especially PhD student Ganesh Vailaya, for their support with equipment and the many engaging scientific discussions that broadened my perspective.

Finally, I am thankful to my family for their endless love and encouragement, which gave me the strength to complete my Master's degree.

Abbreviations

δ – Chemical shift (parts per million)

˚C – Degrees Celsius

aq. – Aqueous

ATR-IR – Attenuated total reflectance infra-red

Calc – Calculated

CV – Cyclic Voltammetry

DMF – N, N-Dimethylformamide

DMAc – N, N'-dimethylacetamide

DMSO – Dimethyl Sulfoxide

eq. – Equivalent

ESI-MS – Electrospray Ionisation Mass Spectrometry

Et_2O – Diethyl Ether

EtOH – Ethanol

HCl – Hydrochloric Acid

Hz – Hertz

IR – Infrared (Spectroscopy)

J – Coupling Constant in NMR Spectroscopy

M – Molar Concentration

m/z – Mass-to-Charge Ratio

Me – Methyl

MeCN – Acetonitrile

MeOH – Methanol

MOF – Metal-Organic Frameworks

NMR – Nuclear Magnetic Resonance

Obs – Observed

POM – Polyoxometalate

PPh_3 – Triphenylphosphine

ppm – Parts per million

RT – Room temperature

TBA – Tetra-n-butylammonium

TEA – Triethylamine

$Zn(OAc)_2$ – Zinc Acetate Anhydrous

Table of Contents

Abstract

Polyoxometalates (POMs) are a group of anionic soluble metal-oxide clusters containing d-block elements in high oxidation states. These compounds are highly valued for their wide range of electrochemical, photochemical, and catalytic properties, due to their remarkable flexibility in tuning both composition and structure. One common method of modifying POM is by connecting the electron-withdrawing organophosphonate groups to the active sites of metal oxides. When POMs are functionalised with organophosphorus compounds, it is possible to adjust their electronic structure and photochemical activity based on the electronic properties of the attached organic moieties. However, the high solubility of POMs restricts their application in sensors, electrodes, and catalysis regions.

By linking POMs in a repeating pattern through bridging organic linkers, insoluble metal-organic frameworks (MOFs) can be formed. These MOFs retain the structural features of the parent molecular POMs and commonly enhance electrochemical activity.

Herein, we report the synthesis of a new hybrid POM, $K_6[P_2W_{17}O_{57}(PO_5H_9C_{13})_2]$ using a biphenyl organophosphonate ligand. The hybrid POMs were characterised by FTIR, NMR and ESI-MS. A series of multi-phenyl organophosphonate functionalised POM were synthesised, and all hybrid POMs were applied to construct POM-based MOFs (POMOFs). The structures of resulting POMOFs were analysed by PXRD. Hybridisation with long-chain organophosphonate groups is expected to stabilise electron-conducting pathways of MOFs, potentially overcoming limitations such as its low conductivity and poor electrochemical durability. The design of these new POMOFs offers a promising strategy for the development of advanced materials for various battery systems.

1. Introduction

1.1 Polyoxometalates

Polyoxometalates (POMs) are a group of soluble anionic metal-oxide clusters, typically composed of $\{MO_x\}_n$ units bridged by oxo ligands.[1,2] These structures feature early transition metals (e.g. M= Mo, W, V or Nb) in their highest oxidation states, resulting in empty d^0 orbitals which allows multi electrons transfer in reactions. POMs exhibit remarkable potential in various regions, including electrochemical,[3,4] photochemical,[5] magnetism,[6] catalytisis[7,8] and medicine.[9] Their broad applicability mainly comes from their structural diversity, highly tunable photochemical and redox activity, and excellent thermal stability.[10,11] Consequently, POMs serve as ideal multifunctional building blocks for the growth of advanced devices and derivative materials.[12]

The development of POM chemistry has a long history, dating back to the first reported POM synthesised by Berzelius in 1826. This historical evolution was comprehensively reviewed by Hill in *Chemical Reviews* (1998),[13] while Pope and Müller's review in the early 1990s helped establish the modern trend of POMs research.[14]

POMs are typically synthesised via a "one-pot" condensation reaction of multiple $\{MO_x\}$ precursors under acidic conditions. Structurally, a classical $\{MO_x\}$ unit consists of a polyhedral anion in which metal cations are coordinated to oxo ligands through M=O or M-O-M linkages. The metal centre is also known as addenda atom, which must retain a high coordination number and form dπ -pπ interactions with oxo ligands. This requirement makes group V and VI transition metals in their highest oxidation states, such as Mo (VI), W(VI) or V(V) the most common choices for constructing $\{MO_x\}$ units. The synthesis of POM could be controlled by varying several parameters: (i) temperature and pressure, (ii) pH and choice of acid, (iii) concentration of metal oxide anions, (iv) ionic strength and reagents equivalent ratio.[15-18]

POMs are broadly classified into isopolyoxoanions and heteropolyoxoanions based on their general structure. Isopolyoxoanions consist of a single type of addenda atom and can be expressed by the general formula $[M_mO_y]^{n-}$ (where M is a highly valent early transition metal). Their archetypal structures—such as the Linqvist ion $[M_6O_{19}]^{n-}$ and its derivatives—are named after the scientists who first characterised their crystal structures. These structures are generally less stable than their hetoropolyoxoanions counterparts.[2] However, advanced studies on

Keplerate-type clusters and other giant POMs have expanded the boundaries of POM chemistry by leveraging vacant d orbital and optimal cation size, particularly from group V and VI elements in the nanoscopic to mesoscopic range.[19, 20] The general formula of Keplerate-type clusters is $[(pentagon)_{12}(linker)_{30}]^{n-}$, where the pentagon unit is $\{M^{VI}{}_6O_{21}\}$ (M = Mo or W). These are coordinated with either monometallic cations (e.g., Fe^{3+}, Cr^{3+}, VO_2^+) or dimolybdic acid unit $\{Mo_2O_2E_2\}^{2+}$ (E= O or S) linker, while the ligands are commonly carboxylates or sulfates.[19, 21, 22]

When hetoroanions such as PO_4^{3-}, SO_4^{2-}, AsO_4^{3-}, SiO_4^{4-}, GeO_4^{4-}, AsO_3^{3-}, SbO_3^{3-} or IO_6^{5-} participate in the self-assembly process, hetoropolyoxoanions are formed. These widely studied POMs are represented by the general formula $[X_xM_mO_y]^{n-}$ and include well-known structures like Anderson-Evans, Keggin or Wells-Dawson types. The Anderson-Evans structure is assembled by six coordinate (octahedral) units, whereas the Keggin and Wells-Dawson types are built from four coordinate (tetrahedral) units.

The joining of p- or d- block heteroatoms can strengthen the structure by filling the external vacancies of lacunary POMs, which are created by removing selected metal centres. These vacant sites can then be substituted with other atoms, allowing precise adjusting the structure and properties of POM. This strategy also facilitates hybridisation, which is a central focus of this thesis.

1.2 Wells-Dawson Polyoxometalates

The typical formula for Wells-Dawson hetoropolyoxoanions is $[X_2M_{18}O_{62}]^{n-}$ (where M= W or Mo), with X is a core heteroatoms that participate in forming the POM structure.[23] The trigonal $[P_2W_{16}O_{62}]^{6-}$ anion was initially described by Wells,[24] and the general formula was later confirmed crystallographically by Dawson in 1953, leading to the Wells-Dawson structure's naming.[25]

The Wells-Dawson POM can be divided into exterior cap positions (located at the top and bottom) and middle belt positions. Functionalisation of the Well-Dawson POM is mainly completed by modifying in the cap position.[26] Comparing with the Keggin structure $[XM_{12}O_{40}]^{n-}$, the Well-Dawson structure can be formed by the dimerisation of two $[XM_9O_{34}]^{n-}$, which is created by the removal of one $\{M_3O_6\}$ unit from the Keggin anion.[27] The two trilacunary Keggin fragments then fuse via

sharing the corner to form the Wells-Dawson anion, which exhibits trigonal symmetry (D_{3h}).

Each $[XM_9O_{34}]^{n-}$ anion comprises a $[XM_3]$ moiety and a $[XM_6]$ moiety, constructing the cap and the belt respectively. Rotational arrangements of these cap and belt positions could give rise to six different isomers, each with distinct stabilities.[28]

Due to its high stability and the structural, electronic and photochemical tunability it offers, the $[\alpha\text{-}X_2W_{18}O_{62}]^{6-}$ species plays an important role in POM chemistry. Over the past decade, Wells-Dawson POMs have shown promise in various biochemical applications, including antibacterial, antiviral, anticancer activities, as well as potential treatments for diabetes.[29-31] In addition, Wells-Dawson POMs are ideal materials for further hybridisation, owing to their relatively stable lacunary structures and high content of addenda atoms.[32]

1.3 Hybridisation of POMs

There has been growing interest in post-functionalisation of lacunary POMs. Organic-inorganic hybridisation is a widely used strategy to tune the physical and electronic properties of POMs, and even to explore novel functionalities by coordinating new ligands at the vacant sites.[33-38]

These organic-inorganic hybrid POMs are typically classified into two types based on the difference of interaction between the POMs and the ligands[1,39]. Class I hybrid POMs interact with organic ligands through non-covalent interactions, for example, hydrogen bonding, van der Waals forces or electrostatic interaction.[40] In contrast, class II hybrid POMs form covalent bonds with their organic ligands. The highly nucleophilic oxygen atoms at the exposed vacant sites of lacunary POMs can form strong covalent interactions with suitable electrophilic centres, such as Si, P and Sn.[40]

Class I hybrid POMs are more extensively studied, primarily because they are easier to synthesise via simple metathesis reactions and are compatible with every anionic POM.[41] A natural example of class I hybrid POMs is found in molybdenum storage proteins, where histidine form strong hydrogen bonds with bridging molybdate oxygen atoms to catalyse condensation reaction.[42] However, the covalent interactions in class II hybrid POMs provide stronger bonding between the POM core and organic ligands, thereby enhancing the stability and resiliency of the resulting

hybrids. This stability enables fine-tuning of electronic and spectroscopic preperties.[43]

Compared to class I hybrids, class II hybrids offer greater tunability, helping to expand more diverse design strategies to functionise materials.[44] Therefore, class II hybrid POMs are often preferred as building units for the assembly of metal-organic frameworks (MOFs).

1.4 Metal-Organic Frameworks & Polyoxometalate-Based MOF

Metal-organic frameworks (MOFs) are a category of crystalline organic-inorganic hybrid polymers formed through self-assembly. The term "MOF" was first named by Yaghi in 1995.[45] Constructed by metal ions or clusters coordinated with organic bridging ligands, these porous materials have become a popular research area in recent years. Interest in MOFs research focuses on the design of structurally predictable frameworks and their applications in gas adsorption and storage,[46] drug delivery,[47] and catalysis,[48,49] due to their high thermal and chemical stability, structures diversity, and large surface area.[50]

MOFs are typically synthesised via hydrothermal methods, although other approaches such as solvothermal,[51] electrochemical,[52] and mechanochemical methods[53] are also used depending on specific requirements.

The design and synthesis of polyoxometalate-based metal-organic frameworks (POMOFs) are developed as an effective strategy to utilise the active sites of POMs.[54] Among the various POM structures, the Keggin and Wells-Dawson types are mainly reported as the choice of POMOF materials. The formation of POMOF combines the high redox activity of POMs with the porosity and tunability of MOFs, resulting in hybrid materials with well-defined structures and enhanced functionalities.[55, 56] Overall, the formation of POMOFs provides a practical method to stabilise the POM structure in solution by reducing its solubility, while simultaneously improving its redox activity.[57.58]

2. Aims

This project aims to investigate the synthesis and characterisation of symmetric organic-inorganic hybrid POMs based on the Wells-Dawson structure, then develops the assembly method to construct POMOFs. Wells-Dawson POMs were selected due to their extensive redox properties and high structural stability.

Firstly, the rod-like electron-withdrawing organophosphonate ligands are used for the hybridisation of Wells-Dawson POMs. These ligands are expected not only to modify the electronic properties of the POM but also to create stronger steric hindrance. This steric effect can tune the reactivity of atoms on the ligand and constrain the 3D extension of the symmetric POM structure, particularly in the horizontal direction.

Secondly, the previously synthesised hybrid POMs will be assembled into POM-organic frameworks (POMOFs). This structural integration is anticipated to enhance the intensity of the parent POMs, decrease its solubility for broader applications, and commonly improve the electrochemical activity of materials.

Finally, to fully characterise the hybrid POMs and POMOFs, several analytical techniques will be employed. These include nuclear magnetic resonance (NMR) spectroscopy, mass spectrometry (MS), and infrared (IR) spectrometry. In addition, electrochemical properties will be investigated using cyclic voltammetry (CV), and the structural features of the resulting POMOFs will be examined by powder x-ray diffraction (PXRD).

3. Results and Discussion

3.1 Synthesis and Characterisation of Polyoxometalate Precursors

To prepare a stable lacunary structure for subsequent hybridisation and MOF assembly, the Wells-Dawson POM $K_6[P_2W_{18}O_{62}]$ (P_2W_{18}) was chosen as the suitable precursor (Figure 1). The P_2W_{18} POMs were synthesised by the "one-pot" reaction under acidic conditions. The sodium tungstate dihydrate dissolved in water as the source of $\{WO_4\}^{2-}$ metal-oxide unit. The dropwise addition of HCl (4M) had two key effects: i) maintaining the pH below 6 prevented degradation of the target Wells-Dawson POM into other lacunary species, and ii) acidifying the solution to pH<2 strongly improved both the yield and purity of the final product.[59,60]

A white precipitate observed during this step was the lacunary intermediate $K_{10}[\alpha_2\text{-}P_2W_{17}O_{61}]\cdot 15H_2O$, which could be redissolved via adding sufficient acid.[61-63] The addition of phosphoric acid provided the PO_4^{3-} anions to participate in the self-assembly of the sandwich-type Wells-Dawson structure. During a 24-hour reflux at 110˚C, the metal-oxide units converted into bimetallic and trimetallic structures. The appearance of a yellow solution indicated the formation of pure $\alpha\text{-}P_2W_{18}$.[64]

After complete conversion, the reaction mixture was cooled down to initiate precipitation of the $K_6[P_2W_{18}O_{62}]$ product. Potassium chloride was added as a counter cation to balance the $[P_2W_{18}O_{62}]^{6-}$ negative charge. The crude product was dissolved in hot water and recrystallised to obtain a product with sufficient yield and purity. Bromine water was added to oxidise the compound from its reduced form. The final product appeared green, which results from a mixture of the yellow $\alpha\text{-}P_2W_{18}$ compound and the heteropoly blues from reduced polyoxometalates.

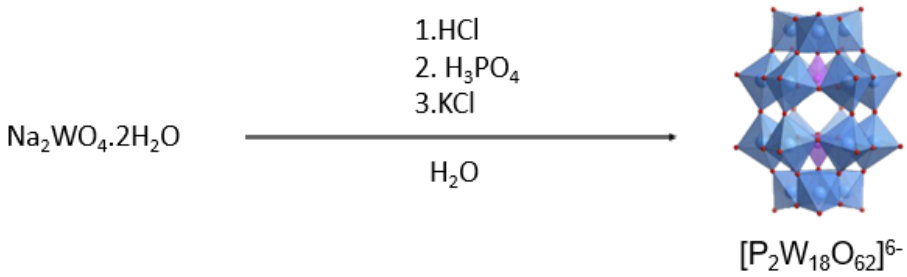

Figure 1: Schematic diagram for the synthesis of the P_2W_{18} POM.

The mono-lacunary Wells-Dawson POM $K_{10}[P_2W_{17}O_{61}]$ (P_2W_{17}) was synthesised for use in hybridisation (Figure 2). As previously mentioned, the P_2W_{18} structure is more stable under acidic conditions. Therefore, to induce the formation of a lacunary site, P_2W_{18} was first dissolved in water and then mixed with potassium bicarbonate to create a basic environment. This decrease in stability let a terminal W=O unit be hydrolysed, generating a vacancy on the POM structure.

The conversion from P_2W_{18} to P_2W_{17} was monitored by the formation of white precipitation after stirring overnight. The precipitation was then dissolved in hot water for recrystallisation and subsequently washed with water and acetone to collect P_2W_{17} product with sufficient yield and purity. The original preparation method was reported by Constant et al in 1990.[65]

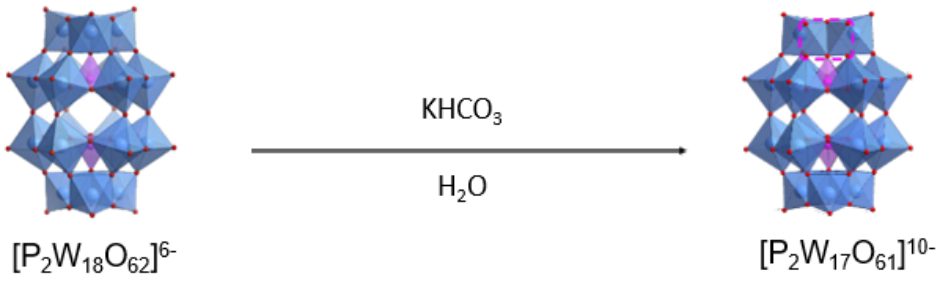

Figure 2: Schematic diagram for the synthesis of the P_2W_{17} lacunary POM.

Phosphorus-31 NMR spectroscopy (^{31}P NMR) was used to characterise the Wells-Dawson POM, providing insights into the environments of the PO_4 units within the POM structure. Compared to other NMR-active isotopes such as ^{17}O and ^{183}W which require specialised setups, including high-resolution spectrometers, high temperature and longer time due to their low natural abundance and low resonance frequency, ^{31}P isotope offers several advantages. It is faster to analyse, more sensitive, and cheaper.[66,67]

In the case of the P_2W_{18} POM, both phosphorus atoms are in chemically equivalent environments, resulting in a single ^{31}P NMR signal. As the comparison, the P_2W_{17} lacunary POM has an asymmetric structure since one W=O unit is removed. This structural change places the two phosphorus atoms in different environments, and thus two distinct peaks are predicted in the ^{31}P NMR spectrum. From the detected ^{31}P NMR spectra a single peak is shown at δ= -13.02 ppm for $K_6[P_2W_{18}O_{62}]$ (P_2W_{18}),

and two peaks are shown at δ= -7.20, -14.38 ppm for $K_{10}[P_2W_{17}O_{61}]$ (P_2W_{17}) (Figure 3). The singlet peak at δ= -7.20 ppm corresponds to the phosphorus atom adjacent to the lacunary site, where a W=O unit has been removed. The absence of nearby W=O unit leads to weaker shielding effect, so the signal of phosphate at the vacant site shifts to downfield. In contrast, the phosphorus atom located farther from the vacant site remains surrounded by more $\{WO_6\}$ units, experiencing greater shielding. As a result, a signal at δ= -14.38 ppm is detected.

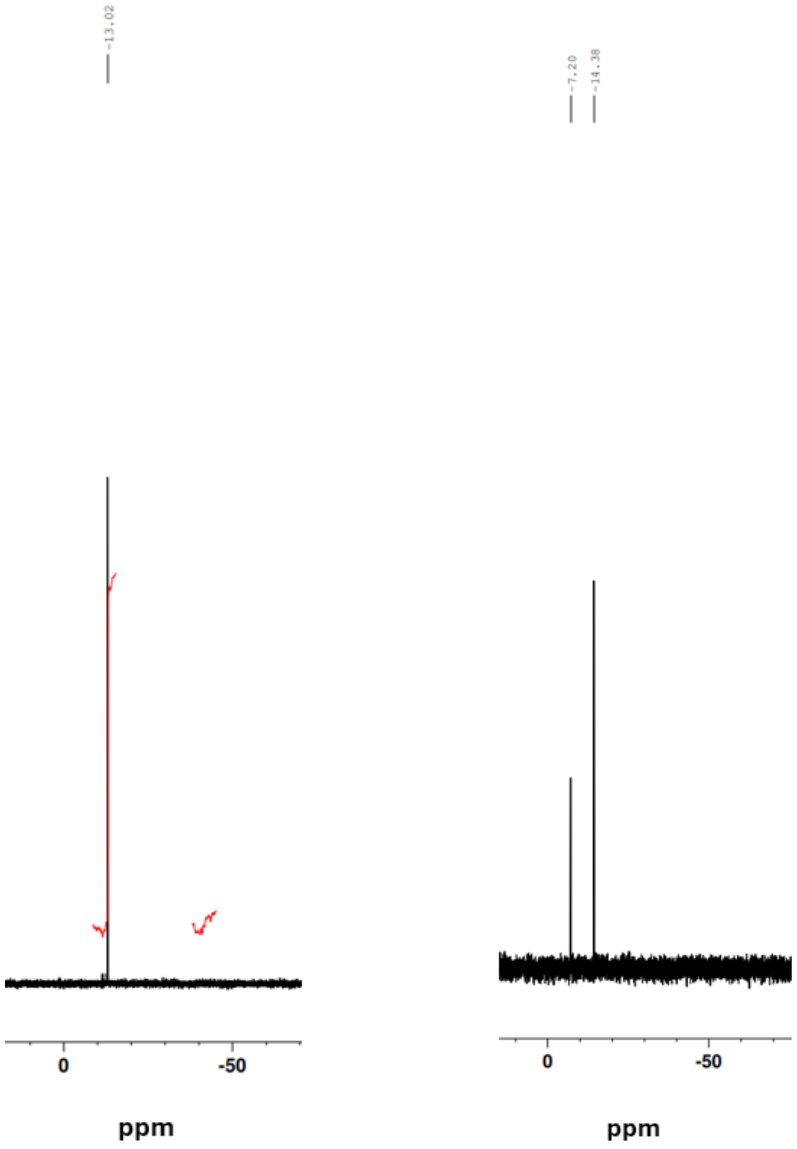

Figure 3: ^{31}P NMR spectra for P_2W_{18} (left) and P_2W_{17} (right) POM in D_2O.

Electrospray ionisation mass spectrometry (ESI-MS) was also employed to support the structural characterisation. The measurements were conducted in Negative High Molecular Weight mode, which is specially optimised for the analysis of large molecules. Several smaller fragments

were identified by ESI-MS to confirm the POM structure. The possible anion assignments for the P_2W_{18} species are presented in Figure 4 and Table 1.

It is worth noting that proton (H^+) and sodium (Na^+) adducts may also be observed because of the working method of ESI technique.[68] In addition, due to the inherently anionic nature of POMs, free exchange of counter cations (e.g., H^+, Na^+, K^+) commonly occurs during the ESI-MS process.[69]

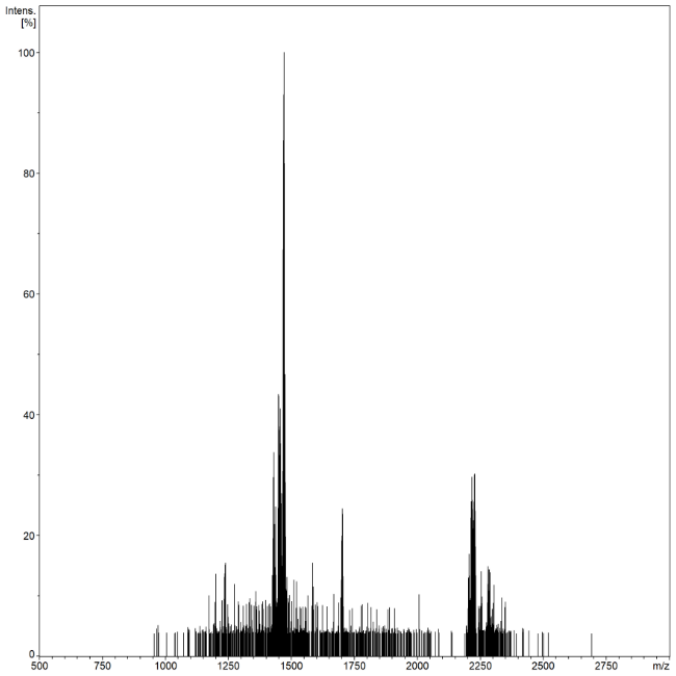

Figure 4: ESI mass spectrum of the P_2W_{18} POM.

Table 1: ESI mass spectrum peak assignments of the P_2W_{18} POM.

Assignment	Z	m/z (obs)	m/z (calc)
$[P_2W_{18}O_{62}]$	3-	1454.90	1454.92
$H_2Na[P_2W_{18}O_{61}]$	3-	1457.91	1457.92
$HNa_2K[P_2W_{18}O_{62}]$	2-	2225.38	2225.37
$H_2NaK[P_2W_{18}O_{61}]$	2-	2214.38	2214.38

ESI-MS was also applied to study the structure of the P_2W_{17} lacunary POM. The detected anion assignments of P_2W_{17} are shown below to support its synthesis (Figure 5 and Table 2).

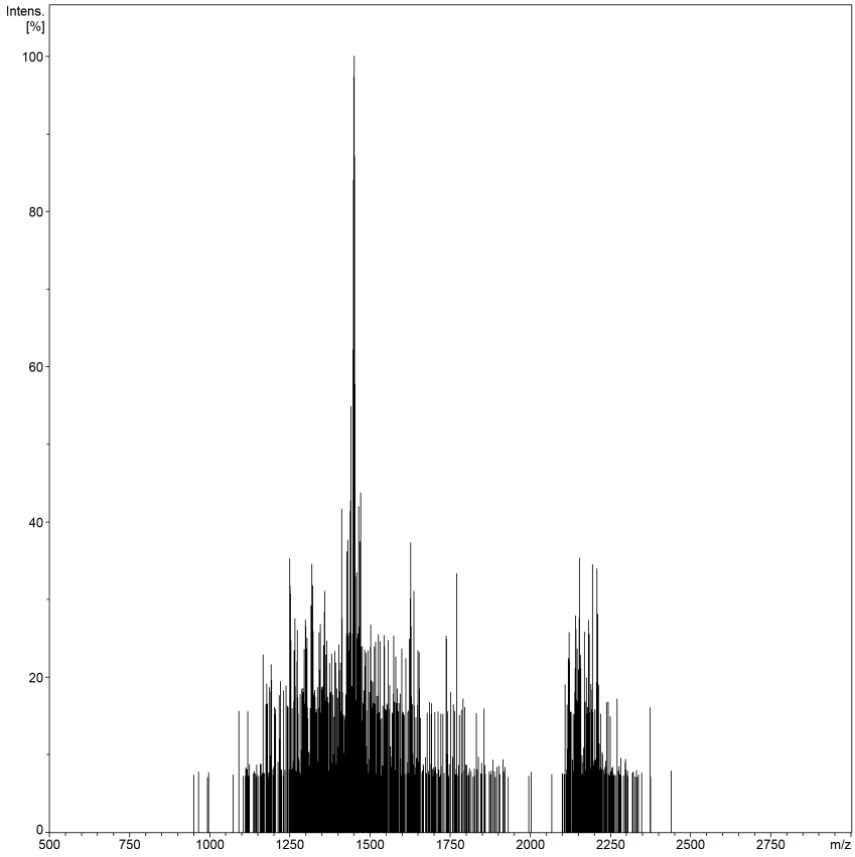

Figure 5: ESI mass spectrum of the P_2W_{17} lacunary POM.

Table 2: ESI mass spectrum peak assignments of the P_2W_{17} lacunary POM.

Assignment	Z	m/z (obs)	m/z (calc)
$HNa_6[P_2W_{17}O_{61}]$	3-	1453.10	1453.05
$H_2Na_5K[P_2W_{17}O_{61}]$	2-	2152.37	2151.36

Infrared (IR) spectroscopy was used to characterise the POMs (Figure 6). Overall, the P_2W_{18} and P_2W17 POM exhibit similar features. A broad peak observed around ~3500 cm^{-1} is assigned to the O-H stretching vibrations. Characteristic POM bands appear in the fingerprint area. The peaks at 1085 cm^{-1} and 1078 cm^{-1} correspond to P-O stretching vibrations of the phosphate units in P_2W_{18} and P_2W_{17}, respectively.[70]

The W=O stretching bonds appear at 956 cm^{-1} for P_2W_{18} and 934 cm^{-1} for P_2W_{17}. The W-O-W bending modes of the bridging oxygens are reported as a broad band: 907-730 cm^{-1} and 515 cm^{-1} for P_2W_{18}, while same mode are identified at 878-715 cm^{-1} and 518 cm^{-1} for P_2W_{17}.[71]

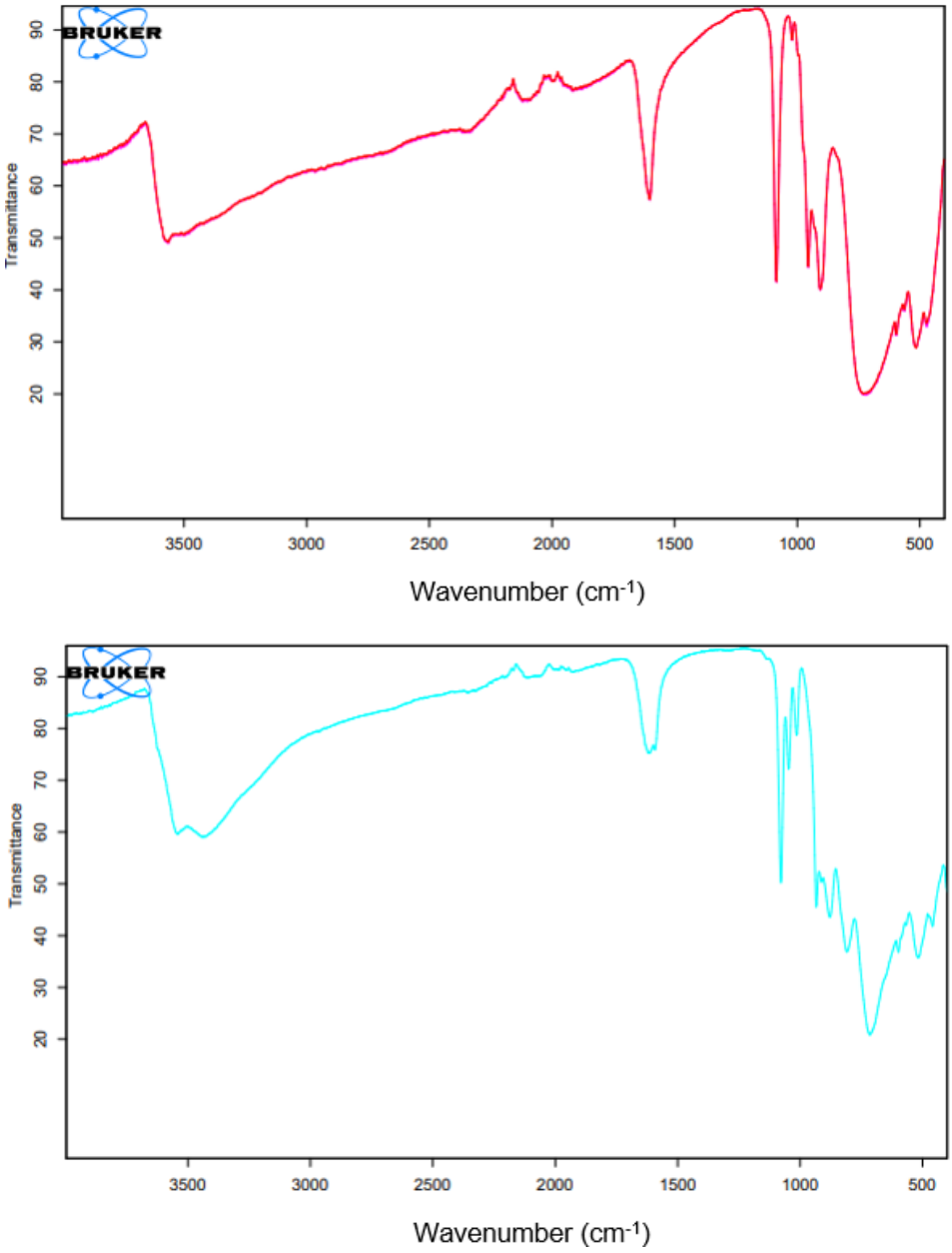

Figure 6: IR (ATR) spectra of the P_2W_{18} (top) and P_2W_{17} (down) POM.

3.2 Synthesis and Characterisation of Symmetric Hybrid POMs

The previously synthesised lacunary Wells-Dawson POM (P_2W_{17}) was used to prepare three kinds of symmetric hybridised POMs. The vacant sites where oxygens are exposed at the edge of the POM structure increased their nucleophilicity. This reactivity allows certain organophosphates to be act as electrophiles ligands. The organo-functionalisation process not only improves the stability and electrochemical properties of the POM but also introduces controllable steric hindrance.

These symmetric organic-inorganic hybrid POM were synthesised individually by acid-catalysed reaction. One molar equivalent of P_2W_{17} was reacted with two equivalents of organophosphonate ligands in acetonitrile. Although the original reported method used DMAc as the solvent, it was replaced with MeCN in this study due to difficulties encountered in collecting sticky, oily products after a few attempts. The detailed synthetic procedures for each hybrid POM are reported in the following sections.

3.2.1 $K_6[P_2W_{17}O_{57}(PO_3H_5C_6)_2]$ (1)

P_2W_{17} POM and phenylphosphonic acid were suspended in acetonitrile, and concentrated hydrochloric acid (12M) was added to facilitate the hybridisation reaction. The mixture was refluxed and stirred at 90 ˚C for 24 hours. After the reaction, unreacted residues were removed by centrifugation. Excess diethyl ether was then added to the liquid mixture to induce precipitation of the hybrid POM, followed by centrifugation. The resulting light green precipitate was resuspended in ethanol and was added excess volume of ether. A second round of centrifugation yielded a light green solid. The reaction scheme is illustrated in Figure 7.

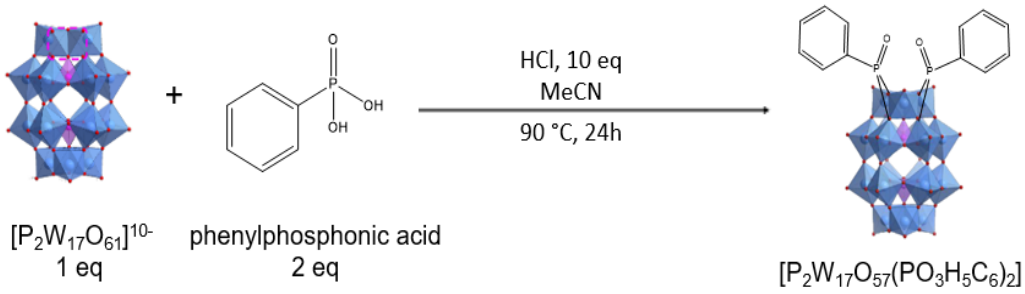

Figure 7: Schematic diagram for the synthesis of the hybrid POM (1).

^{31}P NMR spectroscopy was employed to investigate the phosphate environments in the hybrid POMs, as was done for the parent P_2W_{18} and P_2W_{17} structures. Notably, the appearance of a phosphorus peak in the positive region of the ^{31}P spectrum provides strong evidence to support the formation of hybrid POMs. This is because phosphorus atoms within the POM structure are highly shielded by surrounding $\{WO_6\}$ units. Therefore, symmetric hybrid POMs are predicted to show two peaks in the negative area, corresponding to the two distinct phosphates, and one additional peak in the positive area representing the coordinated phosphonate ligands.

In the case of hybrid POM (1), the ^{31}P NMR spectrum (Figure 8) reveals three distinct peaks: two in the negative area at δ= -11.34 ppm and -12.97 ppm, and one in the positive area at δ= 14.83 ppm, which matches the predicted pattern. The presence of a phosphorus signal at 14.83 ppm represents the coordinated phosphonate ligands. The signal at -11.34 ppm corresponds to the phosphate unit located closer to the top side of the hybrid POM. This unit appeared at -7.20 ppm in the P_2W_{17} spectrum before hybridisation. After coordination, the phosphonate ligands occupy the vacant sites and provide additional electron density, shifting the peak to shielded site.

Conversely, the phosphonic acid ligands also exert an overall electron-withdrawing effect on the hybrid POM. This causes the phosphate unit on the bottom side to become more deshielded.[72] As a result, the corresponding peak shifts to downfield from -14.38 ppm to -12.97 ppm in the hybrid.

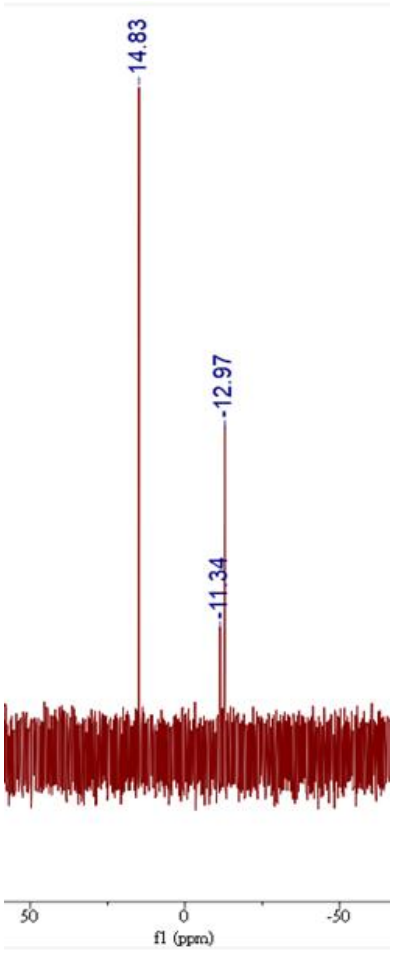

Figure 8: ^{31}P NMR spectrum for hybrid POM (1) in DMSO-d_6.

Proton NMR (^{1}H NMR) was used to analyse the structure of the phosphonate ligands attached to the symmetric hybrid POMs (Figure 9). The key peaks detected in the aromatic area correspond to the aryl groups of the phenylphosphonic acid.[73]

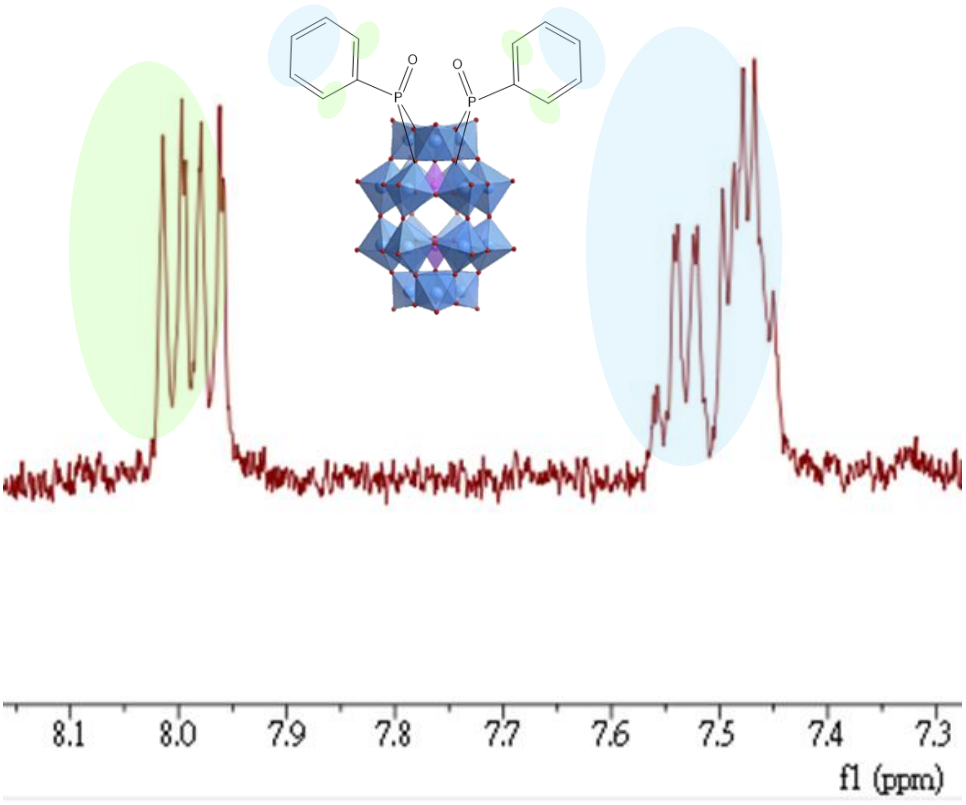

Figure 9: Key sections of ^{1}H NMR spectrum for hybrid POM (1) in DMSO-d_6.

The ESI-MS was used to further investigate the structure of the hybrid POM. As previously mentioned, the presence of proton, potassium and sodium adducts is common in ESI-MS due to the existence of counterions.[68] The measurements were also performed in a Negative High MW mode, and the expected formula for the hybrid POM (1) was $[P_2W_{17}O_{57}(PO_3H_5C_6)_2]^{6-}$. The structure of losing one phosphonate ligand was also considered, since ESI-MS would produce fragments of the molecule. The assignments of hybrid POM (1) are shown below (Figure 10 and Table 3).

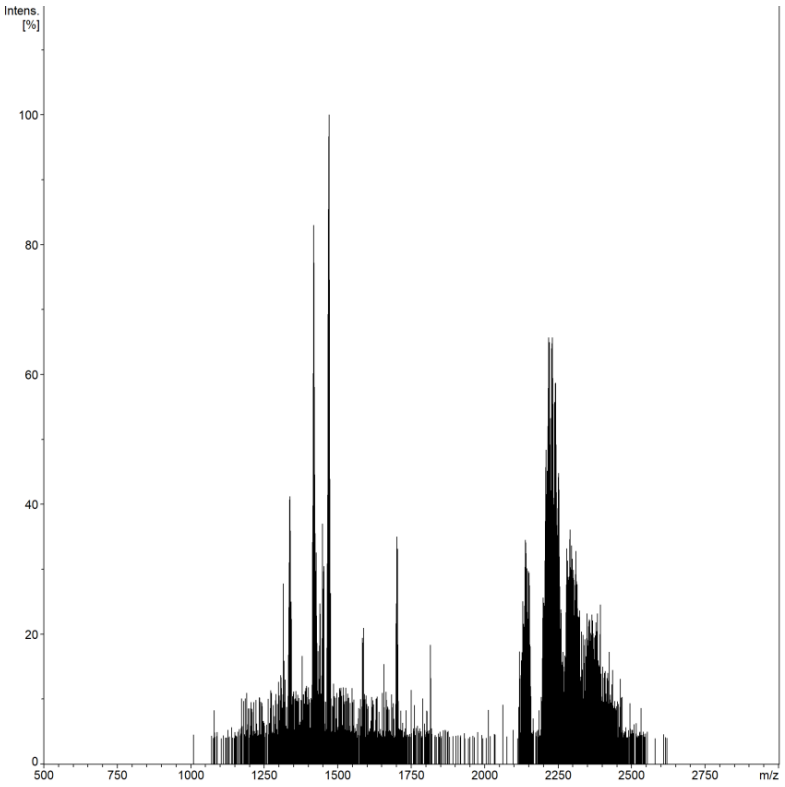

Figure 10: ESI mass spectrum of the hybrid POM (1).

Table 3: ESI mass spectrum peak assignments of the hybrid POM (1).

Assignment	Z	m/z (obs)	m/z (calc)
$H_3[P_2W_{17}O_{57}(PO_3H_5C_6)]$	3-	1419.95	1419.96
$HNa_3[P_2W_{17}O_{57}(PO_3H_5C_6)_2]$	2-	2241.39	2241.40
$H_3K[P_2W_{17}O_{57}(PO_3H_5C_6)_2]$	2-	2227.40	2227.40

Infrared spectroscopy was also used to characterise the hybrid POMs (Figure 11). A broad peak found at ~3500 cm^{-1} is attributed to the O-H stretching from residual moisture. Peaks at 1610 cm^{-1} and 1463 cm^{-1} correspond to C-C stretching vibrations in the aromatic ring of the phosphonate ligand. The characteristic bands of both POM and phosphonate ligand appear in the fingerprint region. A peak at 1086 cm^{-1} indicates the P-O and P=O stretching vibrations from the phosphate units present in both the POM and the ligand. The W=O stretching vibrations are observed at 953 cm^{-1} and 906 cm^{-1}. The W-O-W bending modes of bridging oxygen atoms are reported as a broad band in the range of 725-527 cm^{-1}.

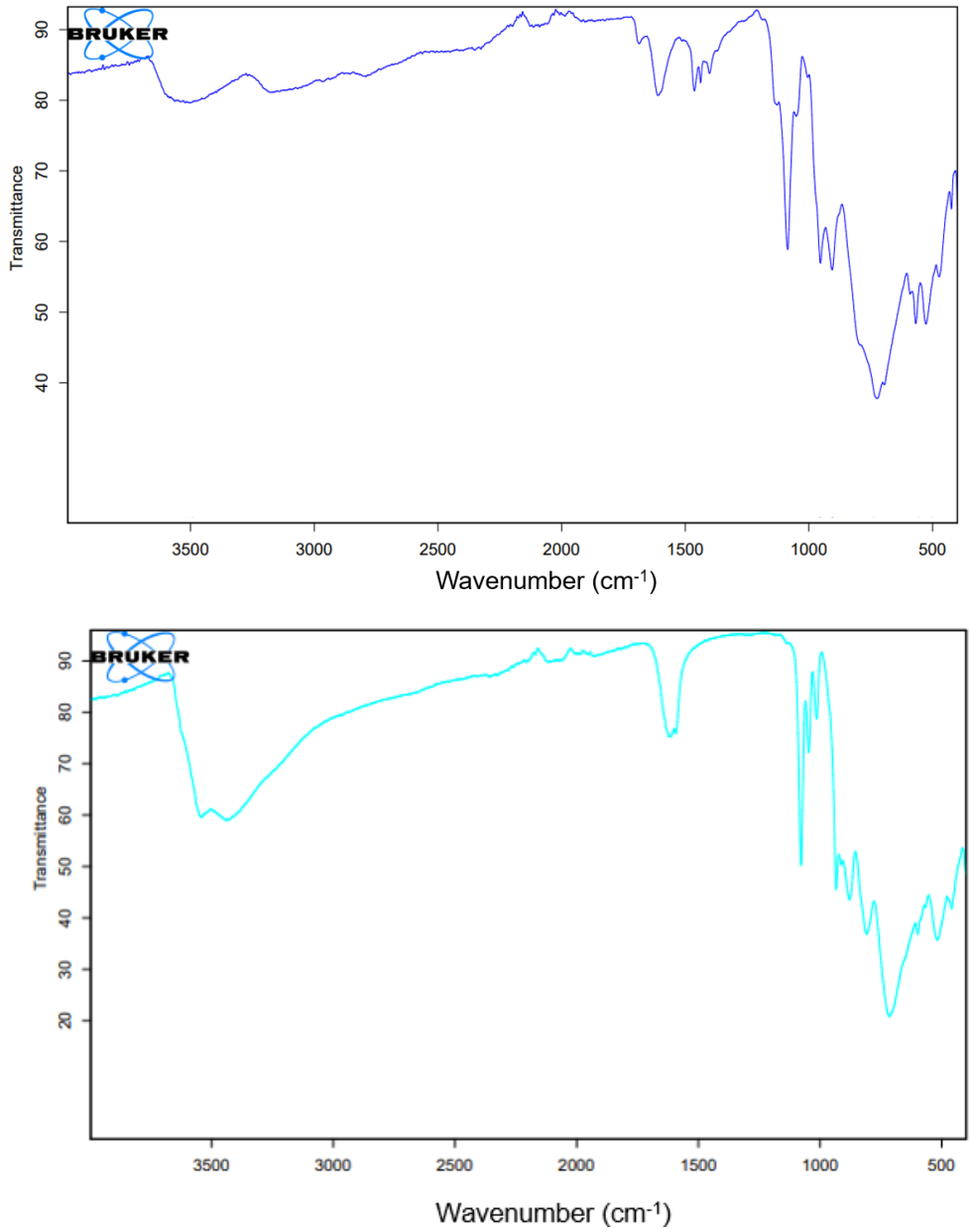

Figure 11: IR (ATR) spectra of the hybrid POM (1) (top) and P_2W_{17} POM (down).

3.2.2 $K_6[P_2W_{17}O_{57}(PO_5H_5C_7)_2]$ (2)

The reaction scheme is shown in Figure 12. The one molar equivalent of P_2W_{17} POM and two molar equivalents of 4-carboxyphenyl phosphonic acid were suspended in acetonitrile. The mixture was refluxed and stirred for at 90 ˚C for 24 hours. After the reaction, unreacted residues were removed by centrifugation, then excess diethyl ether was added to the mixture and centrifuged to precipitate the hybrid POM. The resulting light green precipitate was resuspended in ethanol, followed by the addition of excess ether again, then was centrifugated to collect a light blue solid.

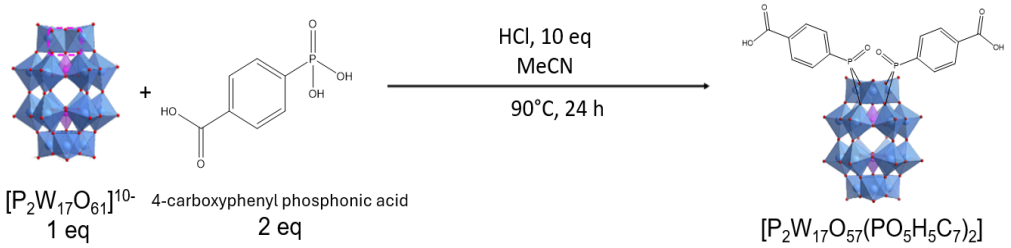

Figure 12: Schematic diagram for the synthesis of the hybrid POM (2).

The ^{31}P NMR spectroscopy was an idea tool for characterising the structures of the hybrid POM (2). It was also used to confirm the formation of hybrid POMs, as the presence of a phosphorus signal in the positive region is indicative of coordinated phosphonate ligands. In hybrid POM (2), three distinct peaks were seen in ^{31}P spectrum (Figure 13): two were at negative region (δ= -11.35, -12.90 ppm) and one was at positive region (δ= 13.28 ppm). This pattern is consistent with the predicted phosphorus environments.

The phosphate unit corresponds to signal at -11.35 ppm is on the top side of the hybrid POM. Compared to the lacunary P_2W_{17} POM, the 4-carboxyphenyl phosphonic acid ligands cause an electron-withdrawing effect on the entire structure. As the result, the phosphate unit located on the bottom side of the hybrid POM becomes more deshielded, leading to a downfield shift of its signal from -14.38 ppm to -12.90 ppm.[72]

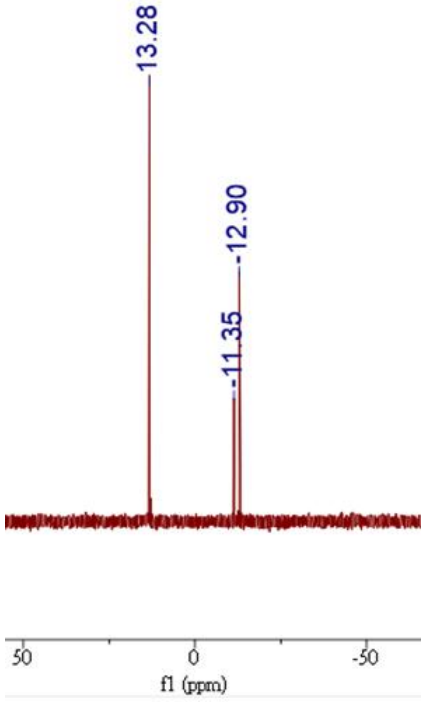

Figure 13: ^{31}P NMR spectrum for hybrid POM (2) in DMSO-d_6.

The proton NMR (^{1}H NMR) was used to identify the structure of phosphonate ligands attached to the symmetric hybrid POMs (Figure 14). A singlet peak observed at 13.17 ppm is attributed to the carboxyl group, while the signals detected in the aromatic region correspond to the aryl group of the 4-carboxyphenyl phosphonic acid ligand.[73]

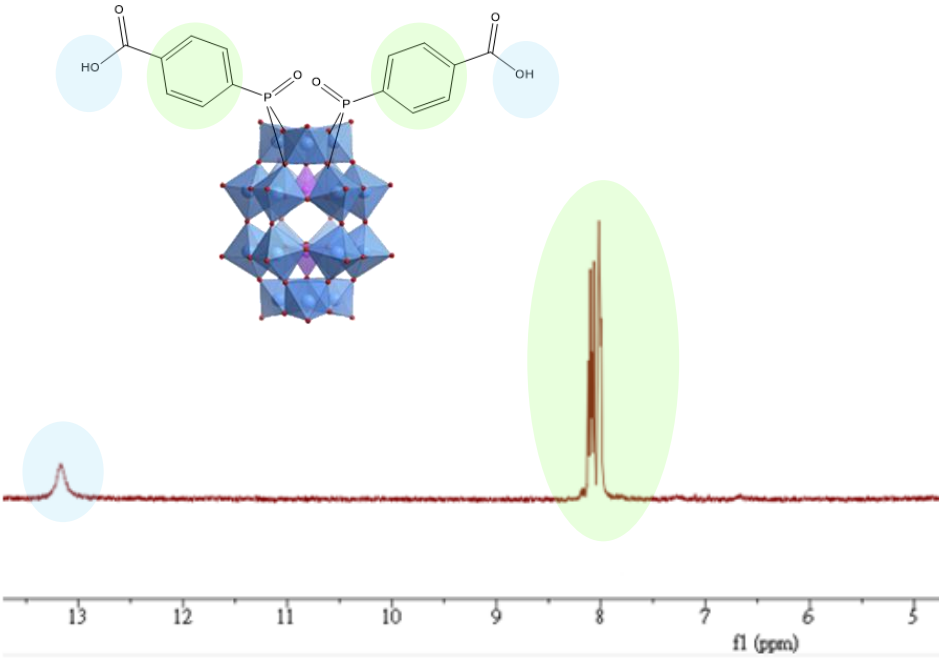

Figure 14: Key section of ^{1}H NMR spectrum for hybrid POM (2) in DMSO-d_6.

The ESI-MS was used to characterise hybrid POM 2 (Figure 15). The expected formula was $[P_2W_{17}O_{57}(PO_5H_5C_7)_2]^{6-}$. The fragment series indicates that the loss of one ligand was also considered in the analysis.

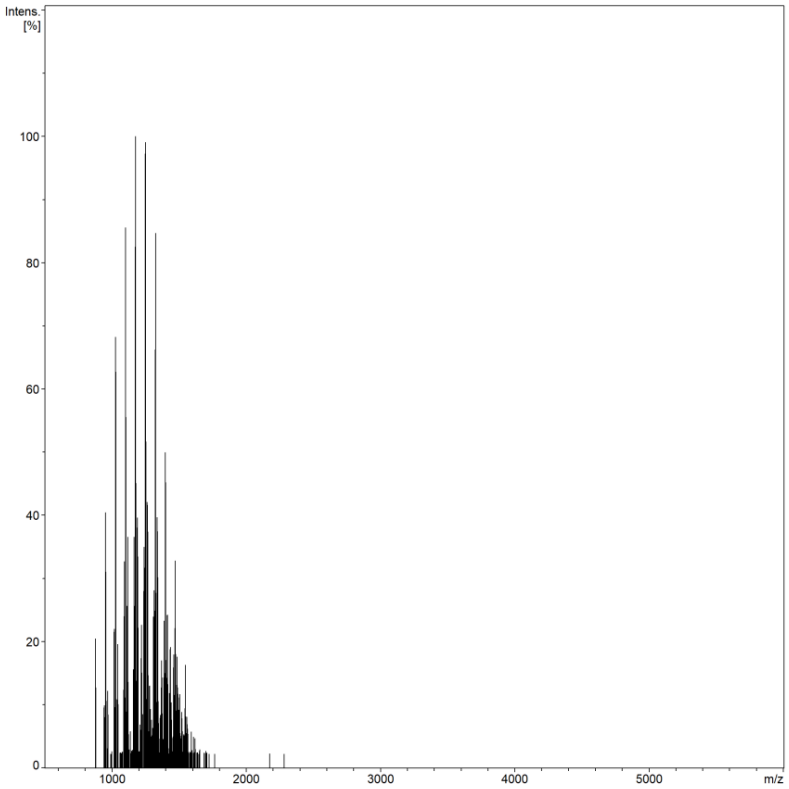

Figure 15: ESI mass spectrum of the hybrid POM (2).

Infrared spectroscopy was used to characterise the hybrid POM (2) (Figure 16). A broad peak found at ~3500 cm^{-1} is assigned to the O-H stretching from residual moisture. The peak at 1701 cm^{-1} corresponds to C=O stretching of the carboxyl group. The peak at 1558 cm^{-1} is attributed to the C-C stretching in the aromatic ring.

The characteristic bands of both the POM and the phosphonate ligand appear in fingerprint region. The peak at 1097 cm^{-1} indicates the P-O and P=O stretching from the phosphate units in both the POM and the ligand. The W=O stretching bonds are observed at 953 cm^{-1} and 914 cm^{-1}. The W-O-W bending modes of bridging oxygen atoms appear as a broad band in the range of 862-531 cm^{-1}.

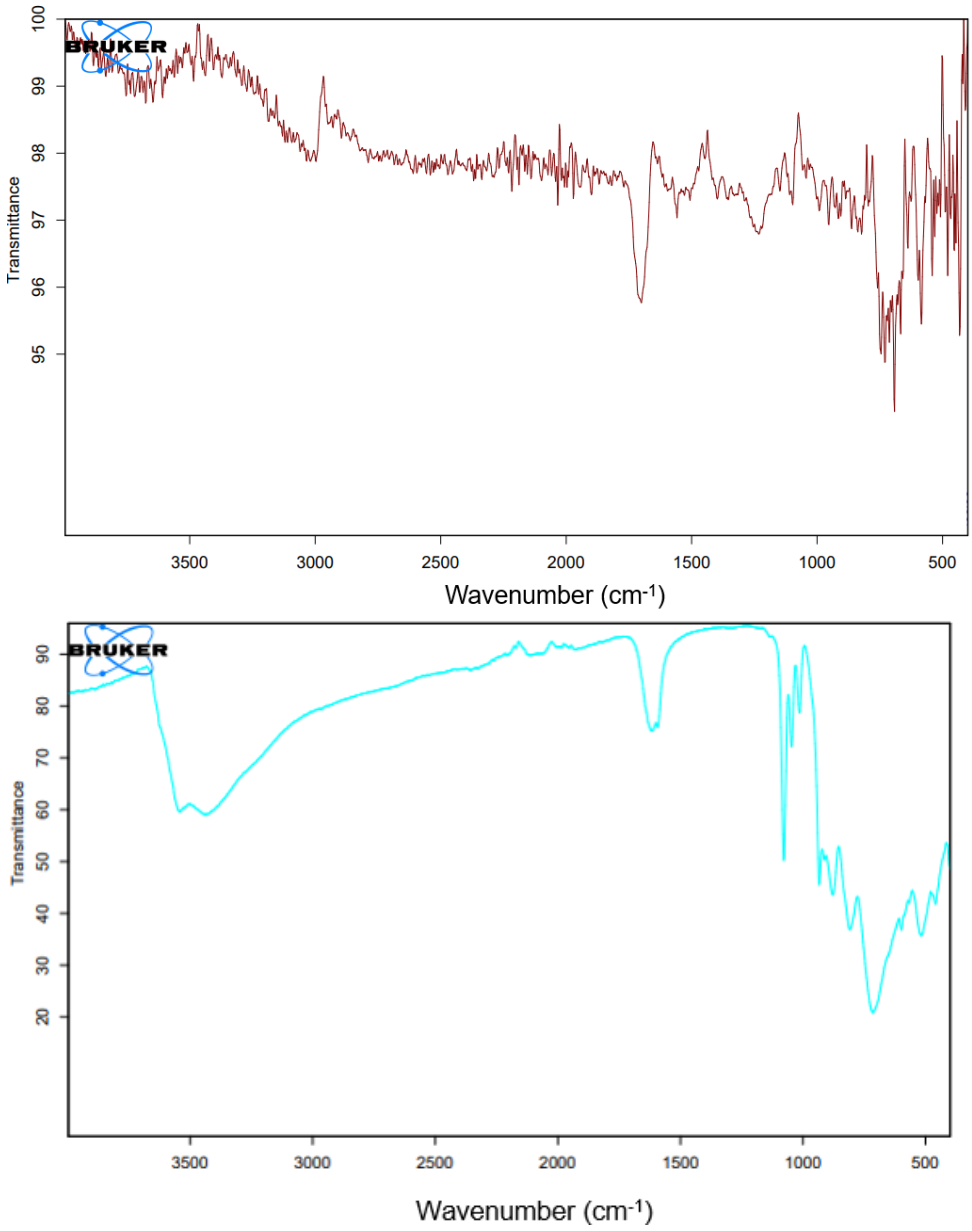

Figure 16: IR (ATR) spectra of the hybrid POM (2) (top) and P_2W_{17} POM (down).

3.2.3 $K_6[P_2W_{17}O_{57}(PO_5H_9C_{13})_2]$ (3)

One molar equivalent of P_2W_{17} POM and two molar equivalents of 4-phosphonato-4'-biphenylcarboxylic acid were suspended in acetonitrile. The mixture was refluxed and stirred at 90 ˚C for 24 hours (Figure 17). The unreacted residue was removed by centrifugation, then excess ether was added to the mixture and centrifuged to precipitate the hybrid POM. The orange precipitate was mixed with ethanol and added excess ether again, centrifuging to collect the final orange solid.

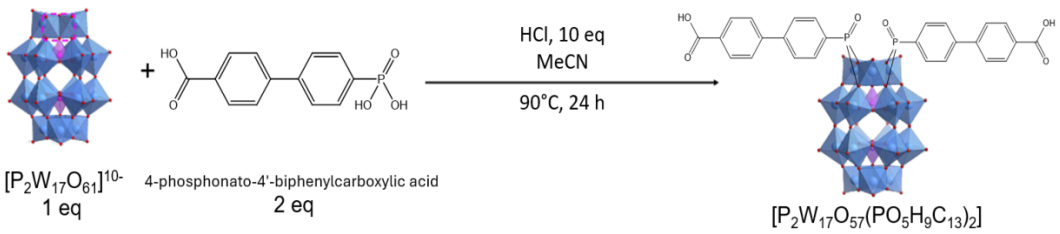

Figure 17: Schematic diagram for the synthesis of the hybrid POM (3).

The structure of the hybrid POM (3) was characterised by ^{31}P NMR spectroscopy. Three distinct peaks are observed in ^{31}P spectrum (Figure 18): two in the negative region (δ= -11.31 and -12.93 ppm) and one in the positive region (δ= 14.57 ppm). The formation of hybrid POM (3) is confirmed by the agreement between the observed peak distribution and the predicted phosphorus environments. The peak at -11.31 ppm corresponds to the phosphate unit located on the top side of the hybrid POM. The 4-carboxyphenyl phosphonic acid ligands cause an electron-withdrawing effect on the hybrid POM, so a downfield shift of the phosphate unit on the bottom side is observed from -14.38 ppm to -12.93 ppm.[72]

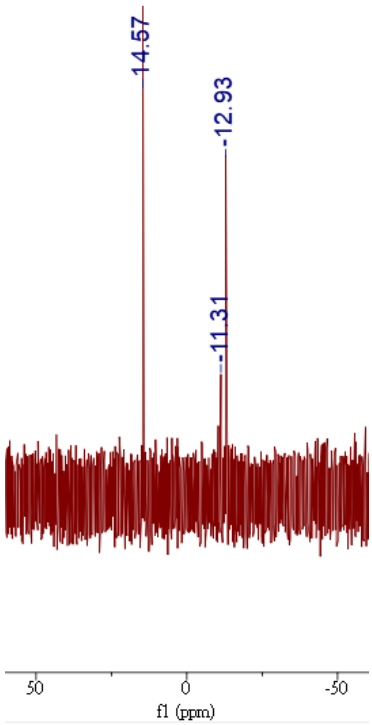

Figure 18: ^{31}P NMR spectrum for hybrid POM (3) in DMSO-d_6.

The proton NMR (^{1}H NMR) was used to confirm the structure of phosphonate ligands attached to the symmetric hybrid POMs (Figure 19). The singlet peak at 12.96 ppm is associated with the carboxyl group, while two multiplets corresponding to the aryl protons indicate the presence of two aromatic rings in 4-phosphonato-4'-biphenylcarboxylic acid.

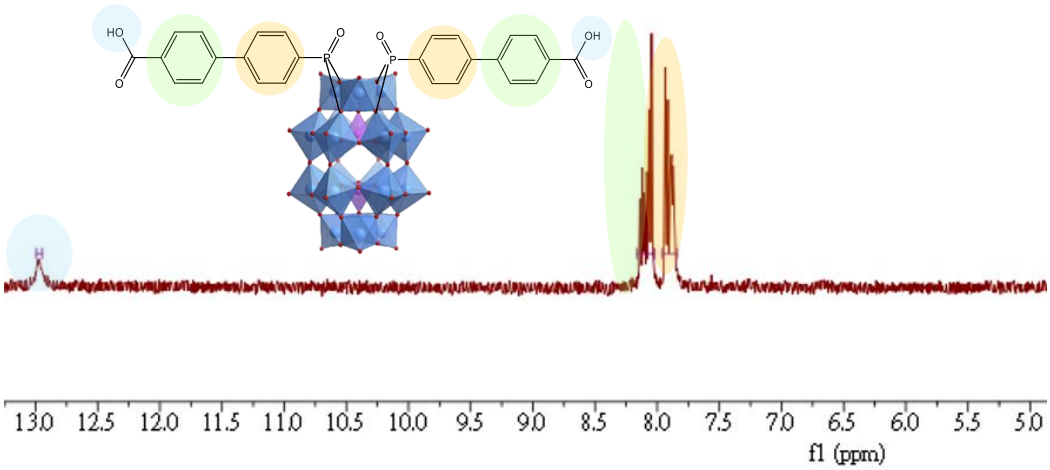

Figure 19: Key section of ^{1}H NMR spectrum for hybrid POM (3) in DMSO-d_6.

The ESI-MS was used to characterise the hybrid POM 2 (Figure 20 and Table 4). The expected formula was $[P_2W_{17}O_{57}(PO_5H_9C_{13})_2]^{6-}$. The fragment series which indicate the loss of one ligand were also considered.

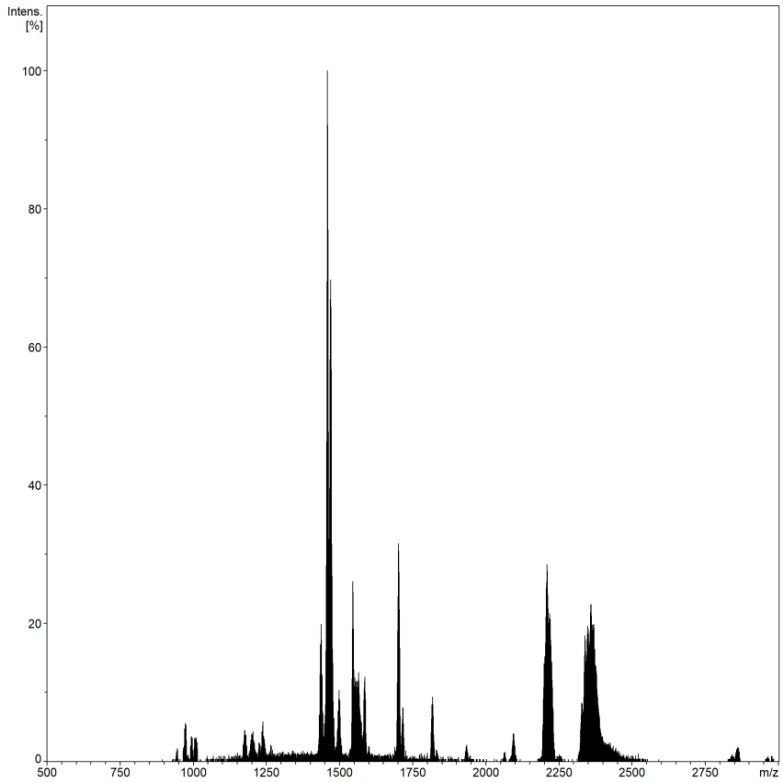

Figure 20: ESI mass spectrum of the hybrid POM (3).

Table 4: ESI mass spectrum peak assignments of the hybrid POM (3).

Assignment	Z	m/z (obs)	m/z (calc)
$H_2K[P_2W_{17}O_{57}(PO_5H_9C_{13})_2]$	3-	1564.73	1564.73
$H_2Na[P_2W_{17}O_{57}(PO_5H_9C_{13})]$	3-	1467.27	1467.29
$H_2KNa[P_2W_{17}O_{57}(PO_5H_9C_{13})_2]$	2-	2358.42	2358.42
$H_2Na_2[P_2W_{17}O_{57}(PO_5H_9C_{13})_2]$	2-	2350.27	2350.27

Infrared spectroscopy was used to characterise the hybrid POM (2) (Figure 21). The peak at 1703 cm^{-1} corresponds to the C=O stretching vibration of the carboxyl group. The peaks observed at 1695 cm^{-1} and 1391 cm^{-1} are assigned to the C-C stretching in the aromatic ring. Characteristic bands of the POM and phosphonate ligand appeared in fingerprint region. The peak at 1086 cm^{-1} is attributed to the P-O and P=O stretching of the phosphate units from both the POM and the ligand. The W=O stretching vibrations appear at 953 cm^{-1} and 907 cm^{-1}. The W-O-W bending mode of the bridging oxygens is reported as a broad band in the range of 721-528 cm^{-1}.

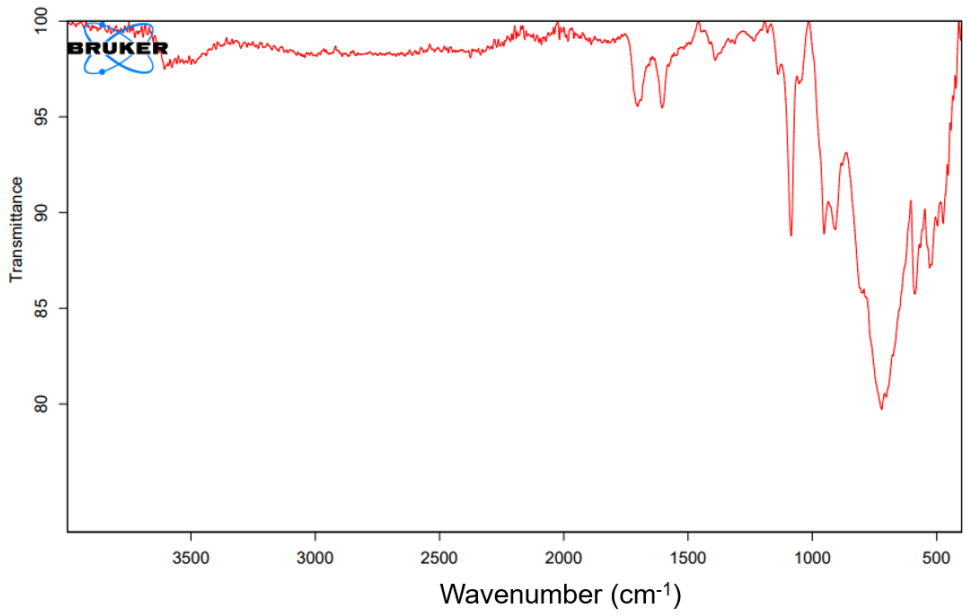

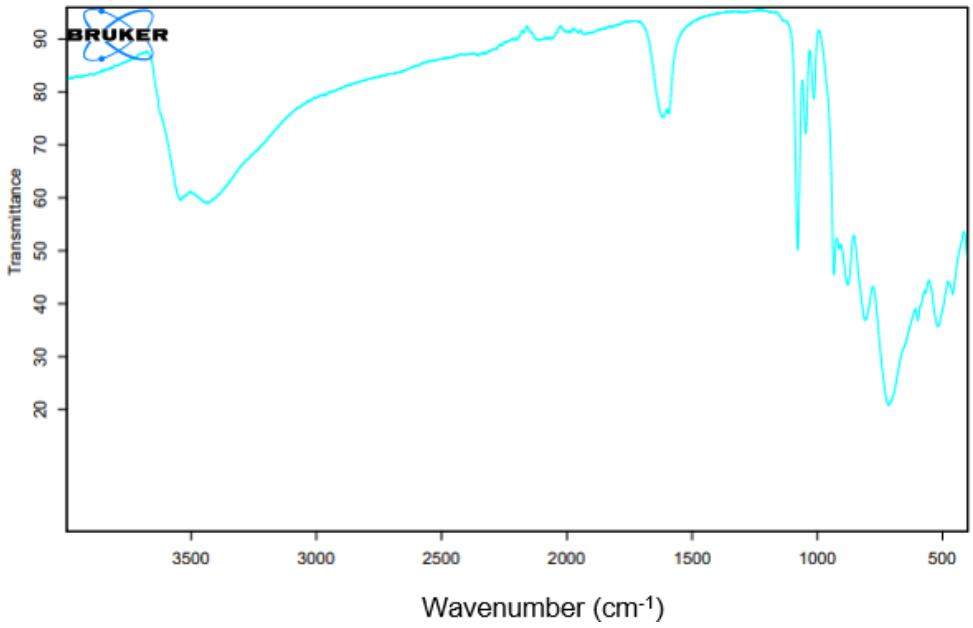

Figure 21: IR (ATR) spectra of the hybrid POM (3) (top) and P_2W_{17} POM (down).

3.2.4 Electrochemistry

Cyclic voltammetry measurements of the P_2W_{18} POM and three hybrid POMs were conducted in MeCN with 0.1 M $TBAPF_6$ as the electrolyte (Figure 22, Table 5&6). For the three hybrid POMs, two distinct redox peaks were observed in the potential range of – 0.9 V to 0 V. In contrast, the P_2W_{18} POM exhibited a broad, poorly defined peak between the range of -1.3 V to 0 V, with a ΔE_p value of 574 mV.

For the hybrid POMs, the first two redox processes (I and II) correspond to single-electron W^{VI}/W^{V} redox processes, with ΔE_p = 72 mV and 74 mV for hybrid POM (1); ΔE_p = 72 mV and 85 mV for hybrid POM (2); and ΔE_p = 89 mV and 95 mV for hybrid POM (3), respectively. Compared with the parent Wells-Dawson POM, the hybrid POMs show a substantial positive shift of around 500- 480 mV. The change of electrochemical properties is due to the electron-withdrawing feature of the organophosphonate linker. In addition, the ΔE_p value for all hybrid POMs exceed 57 mV, indicating that the redox processes are “quasi-reversible” and that electron transfer is electrochemically irreversible under the experimental conditions.

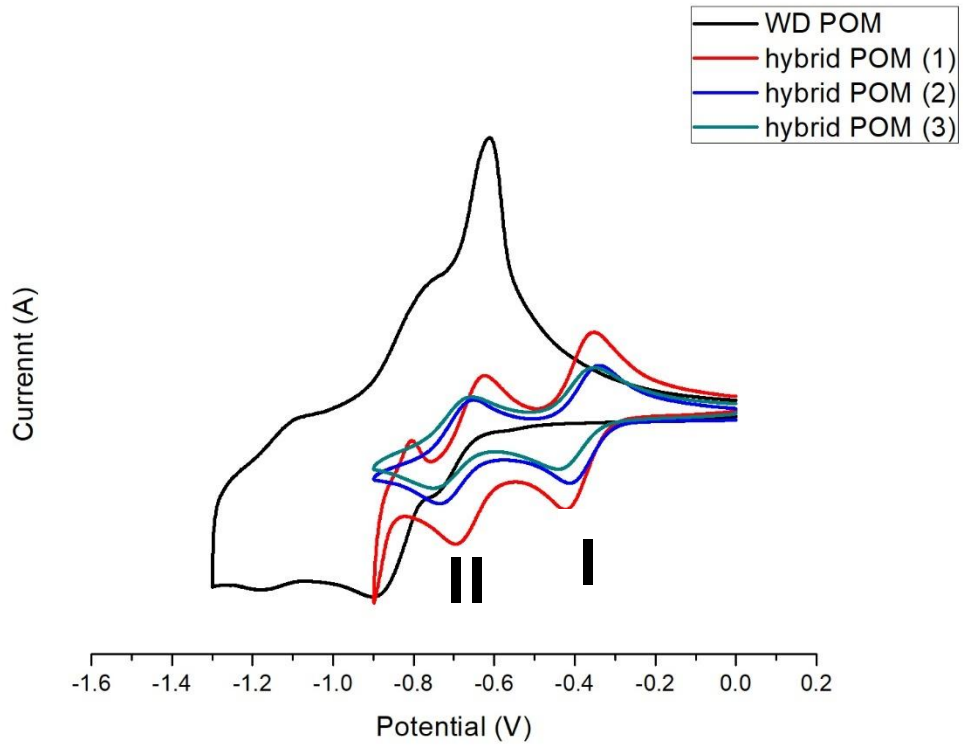

Figure 22: Cyclic voltammograms of the three hybrid POMs and P_2W_{18} POM in MeCN, with 0.1 M $TBAPF_6$. Scan rate: 100 mVs^{-1}

Table 5: 1st redox potential (I) of three hybrid POMs and P_2W_{18} POM in MeCN.

Redox potential vs. Fc/Fc+ (V)	P_2W_{18}	Hybrid POM (1)	Hybrid POM (2)	Hybrid POM (3)
E_{red}	-1.185	-0.424	-0.412	-0.441
E_{ox}	-0.611	-0.351	-0.34	-0.352
$E_{1/2}$	-0.898	-0.388	-0.376	-0.397

Table 6: 2nd redox potential (II) of hybrid POMs (1)-(3) in MeCN.

Redox potential vs. Fc/Fc+ (V)	P_2W_{18}	Hybrid POM (1)	Hybrid POM (2)	Hybrid POM (3)
E_{red}	X	-0.696	-0.735	-0.752
E_{ox}	X	-0.622	-0.65	-0.657
$E_{1/2}$	X	-0.659	-0.693	-0.705

3.3 Attempts Synthesis and Characterisation of POM-based MOF

3.3.1 Hybrid POM (1) cluster

To synthesise a POM-based MOF (POMOF), the linker groups which can work as activation sites on the POM is compulsory. The organo-phosphonate hybridisation is a common method to provide the required components. It is anticipated that the $[P_2W_{17}O_{57}(PO_3H_5C_6)_2]$ (hybrid POM (1)) would be unable to form an extended framework, as it lacks activation sites at positions necessary for self-assembly into a repeating structure.

To test this assumption, a post-functionalisation method was applied to produce a hybrid POM cluster (procedure described in Chapter 5.6). As reported in the literature, the resulting chain-like aggregates still retained the same ^{31}P NMR spectral features as the starting hybrid POM: two peaks in the negative region and one peak in the positive region[74] (Figure 23).

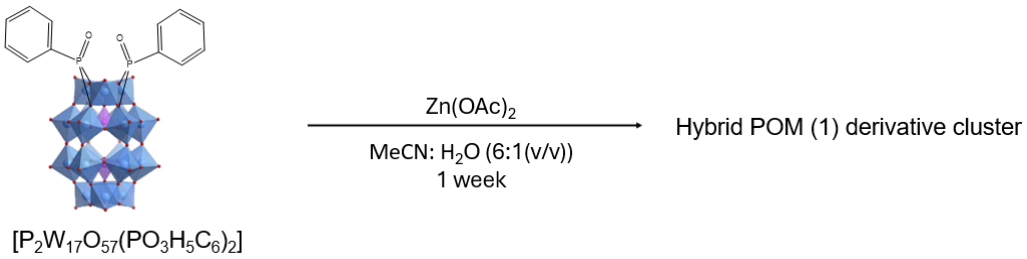

Figure 23: Schematic diagram for the synthesis of the hybrid POM (1) derivative cluster.

For the "clusters" synthesised by hybrid POM (1), all ^{31}P NMR peaks appear the negative region (δ = -9.18, -13.47 and -14.25 ppm) (Figure 24). This spectral pattern does not match the reference, which proves that the hybrid POM (1) fails to form the expected chain-like aggregates. It provides evidence that hybrid POM (1) is unsuitable for constructing a POMOF and should be excluded from the following synthesis attempts. The obvious upfield shift (from 14.83 ppm to -9.18 ppm) suggests that the phosphorus atom in the ligand becomes highly shielded after the reaction. The precise issue of this shift could be discussed in future studies.

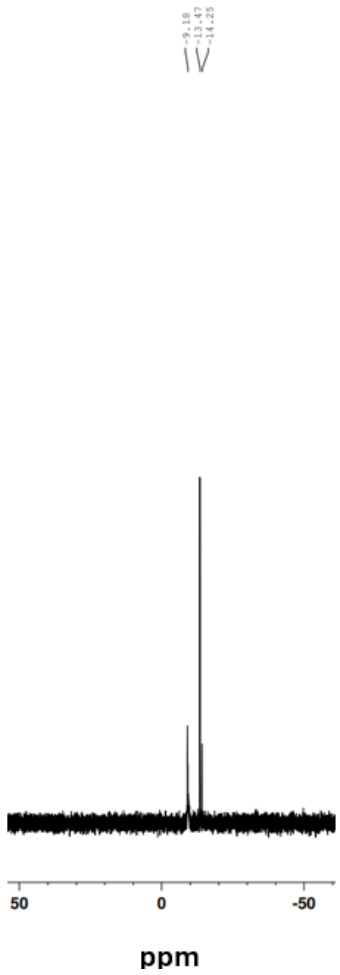

Figure 24: ^{31}P NMR spectrum for hybrid POM (1) cluster in DMSO-d_6

3.3.2 Hybrid POM (2)-MOF

The synthesis of POMOFs was adapted from the MOF-5 preparation method reported by Tranchemontagne, Hunt and Yaghi.[75] One molar equivalent of hybrid POM (2) was dissolved in acetonitrile, then three molar equivalents of triethylamine were added to create a basic reaction environment. Separately, zinc acetate anhydrous (2.5 eq.) was dissolved in a small volume of DMF. The two solutions were combined, stirring for 1 hour, then was left to stand until most of the solvent had evaporated. Ether was added into the remaining solution and sonicated for 10 min, then the ether was replaced with acetonitrile containing a small amount of ether. The mixture was sonicated for a further 5 min, then the product was dried and collected by scraping it from the bottom of the vial (Figure 25).

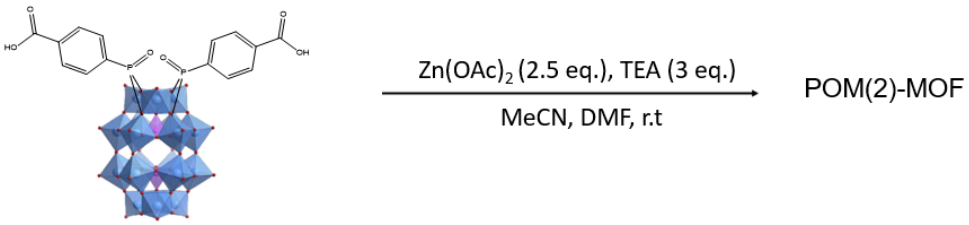

Figure 25: Schematic diagram for the synthesis of the hybrid POM (2) derivative MOF.

The structure of the hybrid POM (2)-MOF was characterised by ^{31}P NMR spectroscopy. Five distinct peaks were observed in the ^{31}P spectrum (Figure 26), three are in the negative region (δ= -3.08, -11.30, -13.04 ppm) and two in the positive region (δ= 10.38 and 0.26 ppm). The phosphate units corresponding to the reactant hybrid POM (2) can be identified at δ= 10.48, -11.30, -13.04 ppm. Compared with hybrid POM (2), the peak originally at 13.28 ppm shifted to 10.38 ppm after the reaction, indicating an increase in election density at the phosphorus atom of the ligand. The overall POM structure provides a stronger shielding effect, and the peak corresponding to the bottom phosphonate unit moves to upfield (from -12.90 ppm to -13.04 ppm). The peaks at 0.26 ppm and -3.08 ppm indicate the presence of small fragments dissociated from the hybrid POM. These fragments are likely produced by degradation, in which W=O or W-O-W bonds are attacked by the nucleophile, generating more vacancies.[76,77] The resulting small species aggregate into a brown, gel-like material. The poor solubility of the product in MeCN, MeOH and water makes the common ESI-MS solvent unusable for structural analysis.

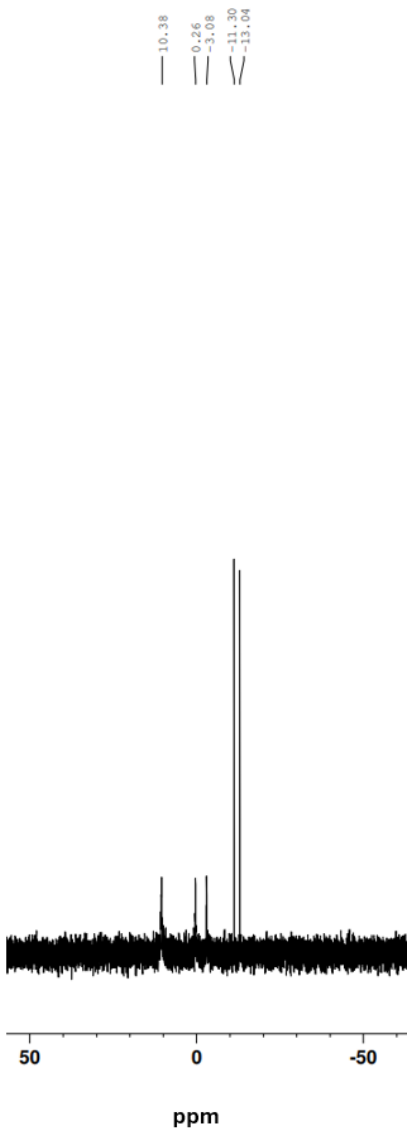

Figure 26: ^{31}P NMR spectrum for hybrid POM (2)-MOF in DMSO-d_6.

3.3.3 Hybrid POM (3)-MOF

The first attempt to synthesise the POM (3)-MOF followed the procedure described in 3.3.2. However, a brown jelly was formed when the same amount of TEA was mixed with hybrid POM (3) in MeCN during the experiment, which was insoluble in additional MeCN (Figure 27). This outcome was attributed to base-induced degradation. To solve this issue, the reaction conditions were modified using two alternative methods. In Method A, 2 equivalents of acetic acid were added to lower the pH. In Method B, the amount of TEA was simply reduced.

Figure 27: The jelly formed after TEA was added in the hybrid POM (3)/ MeCN solution.

Method A: One molar equivalent of hybrid POM (3) was dissolved in acetonitrile, then three molar equivalents of TEA were added to create a basic reaction environment. A brown gel-like material formed in the vial, after which 2 equivalents of acetic acid were added to re-dissolve the gel. Zinc acetate anhydrous (2.5 eq.) was dissolved in a small amount of DMF, and the two solutions were combined and stirred before being left to allow solvent evaporation. Ether was then added, and the mixture was sonicated. The ether was subsequently replaced with acetonitrile containing a small amount of ether, and the mixture was sonicated for an additional 5 minutes. The final product was dried and collected (Figure 28).

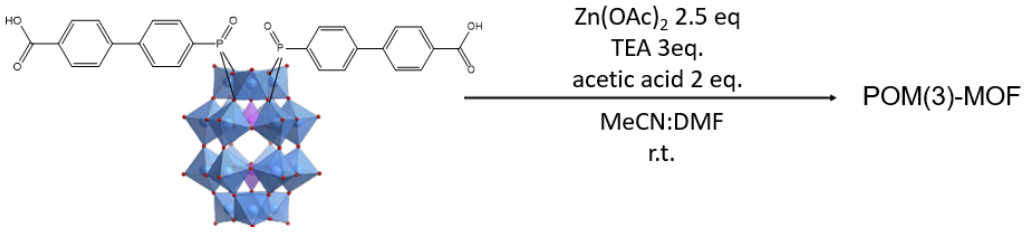

Figure 28: Schematic diagram for the synthesis of the hybrid POM (3) derivative MOF with method A).

Method B: One molar equivalent of hybrid POM (3) was dissolved in acetonitrile, followed by the addition of reduced amount of TEA (0.75 eq) to provide a basic reaction environment. In this case, no brown gel-like material was formed. Zinc acetate anhydrous (2.5 eq.) was dissolved in a small amount of DMF, then two solutions were combined and stirred before being left to allow solvent evaporation. Ether was then added for

sonication, replaced with acetonitrile containing a small amount of ether. The mixture was sonicated for an additional 5 minutes, then the final product was dried and collected (Figure 29).

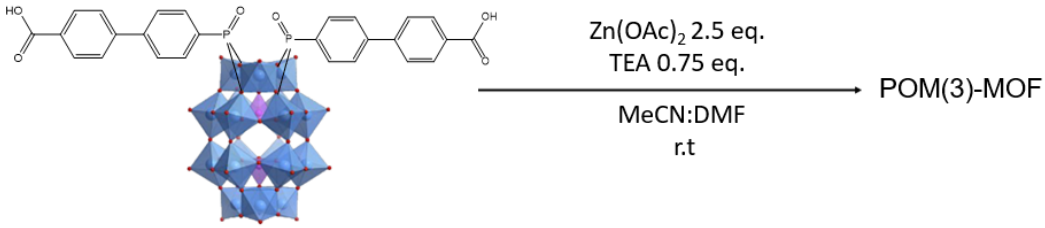

Figure 29: Schematic diagram for the synthesis of the hybrid POM (3) derivative MOF with method B).

The structure of hybrid POM (3)-MOFs synthesised by Method A and B were characterised using ^{31}P NMR spectroscopy. The products obtained from each method are named according to the method used. For both Product A and Product B, three distinct peaks were observed in ^{31}P spectra (Figure 30): two in the negative region (δ= -11.28 and -13.05 ppm for Product A; δ= -11.27 and -13.04 ppm for Product B) and one in the positive region (δ= 10.80 ppm for Product A; δ= 10.65 ppm for Product B). These peaks highly correspond to those of the reactant hybrid POM (3).

Compared with hybrid POM (3), the peak at 14.57 ppm shifts to 10.80 ppm (A) or 10.65 ppm (B), indicating an increase in election density at the phosphorus atom of the ligand. No peaks corresponding to small fragment species were detected in spectra, proving that base degradation was controlled in both methods. Furthermore, the upfield shift of the bottom phosphonate unit (from -12.93 ppm to -13.05 for A/ -13.04 ppm for B) reflects an increased shielding effect from the POM. This points out that the whole POM structure was modified or assembled into larger molecules through self-organisaton. The poor solubility of both products in MeCN, MeOH and water makes the conventional ESI-MS solvents unsuitable for structural analysis.

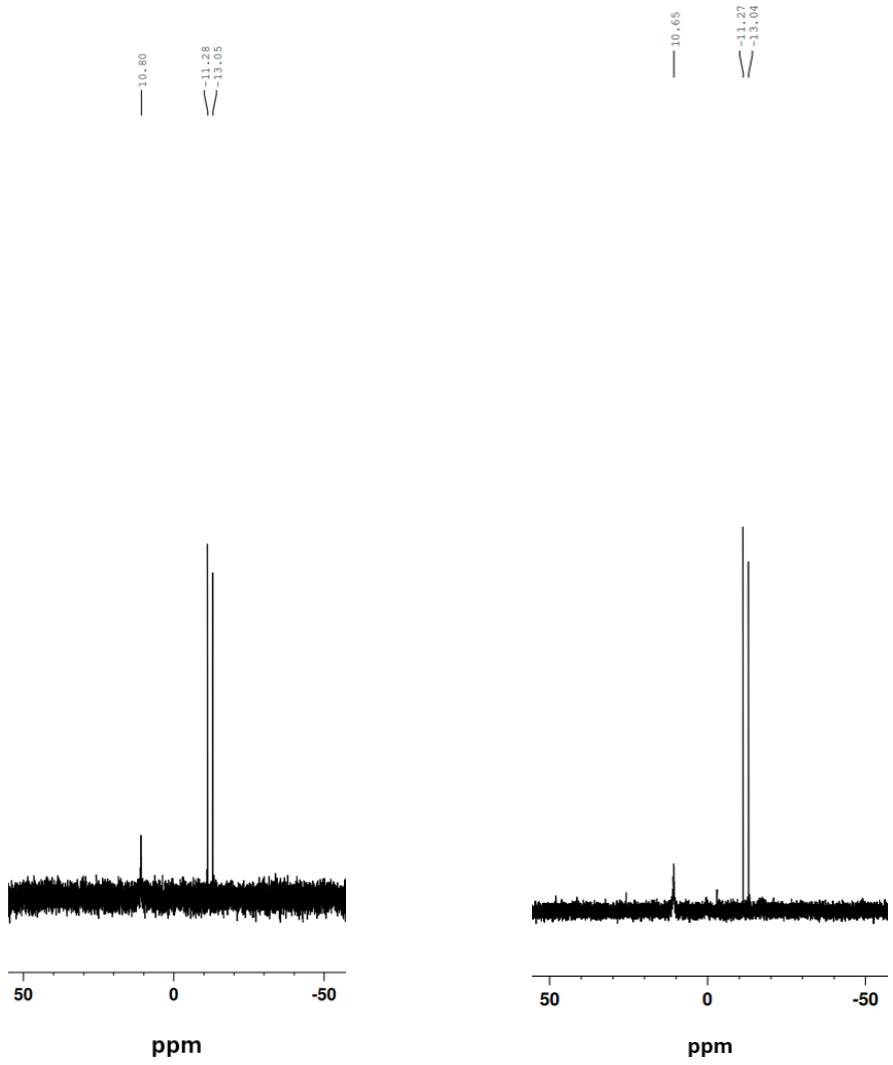

Figure 30: ^{31}P NMR spectra for product A (left) and product B (right) of hybrid POM (3)-MOF in DMSO-d_6.

3.3.4 Powder X-ray Diffraction

Powder X-ray diffraction (PXRD) is a widely used technique for characterising nanoscale materials, providing essential information on crystallinity, structural details, particle size and sample purity. The PXRD results indicate that most of the synthesised samples do not have enough crystallinity to observe peak positions when compared with the pattern of MOF-5, instead displaying wavy curves (Figure 31). Therefore, it is difficult to determine whether the target POMOFs adopt a true MOF structure or represent other types of species. Further recrystallisation will therefore be necessary. In addition, the synthesised MOF-5 was analysed in its inactive state. Its PXRD pattern does not match the standard database pattern, likely because the porous structure is filled with residual solvent or zinc oxide. The synthetic procedure for MOF-5 is described in Chapter 5.6.

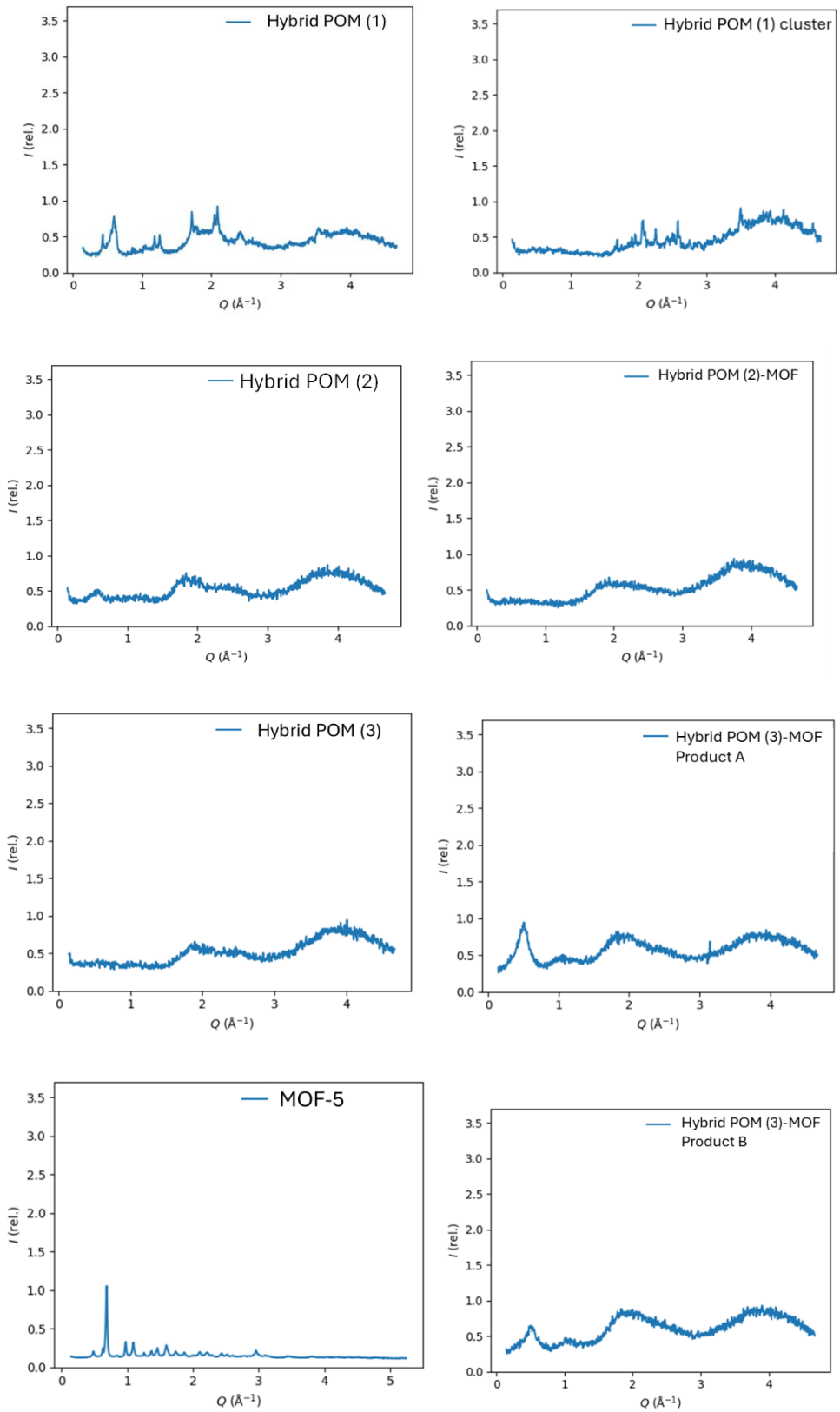

Figure 31: PXRD pattern for hybrid POMs, MOF-5 and hybrid POMOFs.

4. Conclusions and Future Work

A new symmetric hybrid POM [$P_2W_{17}O_{57}(PO_5H_9C_{13})_2$], based on 4-phosphonato-4'-biphenylcarboxylic acid, has been synthesised and characterised. Three symmetric hybrid POMs were used as structural units for the construction of MOFs framework, and their electrochemical properties were investigated. Several MOF synthetic methods were explored. The structural information for both hybrid POMs and POMOFs was obtained via PXRD. However, the crystallinity of the samples was insufficient for detailed structural analysis.

After POMOF formation, all compounds exhibited reduced solubility, which matched the expectation that MOF assembly could enhance the stability of hybrid POMs in various solvents. This increased stability explores potential usages in heterogeneous catalysis, novel solid materials, and energy storage. Nonetheless, further analysis is required to define the precise formulas of these materials.

Due to time restrictions, synthetic methods for using more rod-like oligophenyl phosphonate ligands were not developed. To examine the influence of steric hindrance on POMOF formation, longer phosphonate ligands could be used in future hybridisation studies. The formation of a brown gel-like material is a unique phenomenon observed exclusively when hybrid POM (3) is used in POMOF synthesis, and this substance could be further characterised for its structure and potential applications. Other reaction conditions could also be tested to optimise POMOF synthesis, ranging from simply changing the reaction temperature and pressure to utilise alternative synthetic methods.

5. Experimental

5.1 Materials and Methods

All common reagents and solvents were purchased from commercial suppliers and used without further purification.

NMR Spectroscopy: ^{1}H, ^{31}P and ^{13}C NMR spectra were measured in DMSO-d_6 with a Bruker Ascend™ 400 MHz spectrometer. Chemical shifts (δ) are reported in parts per million (ppm).

Fourier Transform Infrared Spectroscopy (FTIR): IR spectra were recorded in the range 4000-400 cm^{-1} on a Bruker Alpha FTIR spectrometer equipped with a platinum ATR module.

Electrospray Ionisation Mass Spectrometry (ESI-MS): High-resolution ESI-MS measurements were performed on a Bruker micrOTOF II mass spectrometer, operated in negative ion mode unless specifically noted. Samples of organophosphonate ligands and their precursors were prepared in methanol, while POM samples were prepared in acetonitrile, each at a concentration of approximately 0.01 mg mL^{-1}.

Powder X-ray Diffraction (PXRD): PXRD patterns were recorded on a Malvern PANalytical Xpert Pro MPD (Cu source). All samples were analysed over a of 2°-70° diffraction angle with a 30-min step time, repeated 4 times. For MOF-5, data were collected under these parameters: 2°-80° diffraction angle and 10-min step time scanning.

Cyclic Voltammetry (CV): CV measurements were performed on a CHI600E workstation using a three-electrode system: a glassy carbon working electrode, a platinum wire counter electrode, and an Ag/AgCl reference electrode. A 0.1 M $TBAPF_6$ in acetonitrile was used as the electrolyte solution. All measurements were performed after degassing with argon for 15 min and under a positive argon atmosphere. The scan rate during measurements was 100 mVs^{-1}.

5.2 Synthesis of Organophosphonate Ligand

5.2.1 Synthesis of 4-Diethylphosphono-4'-Biphenylcarboxylic Acid Methyl Ester

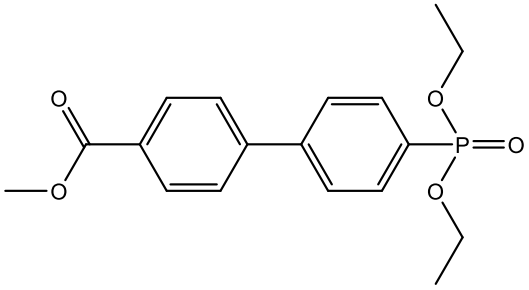

Methyl 4-(4’-bromophenyl) benzoate (400 mg, 1.38 mmol), PPh_3 (106.8 mg, 0.408 mmol) and $Pd(OAc)_2$ (31.6 mg, 0.141 mmol) were suspended in ethanol (17 mL) under argon. Diethyl phosphite (710 µL, 5.64 mmol) and triethylamine (580 µL, 4.17 mmol) were added. The reaction mixture was refluxed at 75 ˚C for 22 h and subsequently cooled to room temperature. The yellow solution was centrifuged to remove solids, and the solvent was evaporated under reduced pressure to form a yellow precipitate. The crude product was extracted with dichloromethane and washed three times with water. The organic phase was collected, and the solvent was removed under vacuum to yield a light-yellow product (529 mg, 110%).[78,79]

^{1}H NMR (400 MHz, DMSO-d_6):

δ = 8.12 - 7.79 (m, 8H), 4.05 (q, *J* = 3.6 Hz, 4H), 3.90 (s, 3H), 1.26 (t, *J* = 7.1 Hz, 6H).

^{13}C NMR (101 MHz, DMSO-d_6):

δ = 166.4 (-COOH), 143.9 (aromatic C), 143.1, 132.6, 132.5, 132.0, 131.9, 130.4, 129.7, 129.6, 129.3(d), 127.8 (d), 62.3 (O-CH_3), 52.7 (O-CH_3), 16.7(-CH_3).

^{31}P NMR (162 MHz, DMSO-d_6):

δ = 17.52.

MS (ESI): Calc for $[C_{18}H_{21}O_5PH]^+$ m/z = 349.1199. Found=349.1202 (measured with positive mode).

5.2.2 Synthesis of 4-Phosphonato-4'-Biphenylcarboxylic Acid

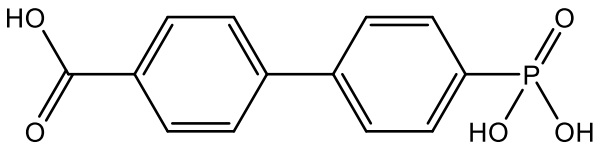

4-diethylphosphono-4’-biphenylcarboxylic acid methyl ester (200 mg, 0.574mmol) was suspended in HCl (12 M, 15 mL) and refluxed at 90 ˚C for 20 h. The resulting yellow mixture was cooled in an ice bath then filtered. The solid was washed with plenty of water to remove excess HCl. After filtering under vacuum, the light-yellow precipitate was obtained and dried to yield the final product (119 mg, 75%).[79]

^{1}H NMR (400 MHz, DMSO-d_6):

δ =8.05 (d, *J*=8.4 Hz, 2H), 7.89 - 7.74 (m, 6H). (The broad peak from P-OH bond was not visible). [79]

^{13}C NMR (101 MHz, DMSO-d_6):

δ = 167.5 (-COOH), 144.0 (aromatic C), 131.8, 131.7, 130.6 130.5, 127.5, 127.2, 127.1.

^{31}P NMR (162 MHz, DMSO-d_6):

δ = 12.27.

MS (ESI): Calc for $[C_{13}H_{10}O_5P]^-$ m/z = 277.0271. Found= 277.0271

5.3 Synthesis of Polyoxometalates

5.3.1 Synthesis of $K_6[P_2W_{18}O_{62}]$ (P_2W_{18})

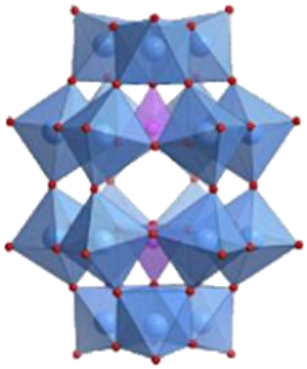

The classic Wells-Dawson POM was prepared following the method reported by Graham and Finke.[63]

$Na_2WO_4{\cdot}2H_2O$ (50.0 g, 0.152 mol) was dissolved in water (60 mL), and HCl (4 M, 42 mL) was added dropwise to the solution under rapid stirring. A white precipitate formed during the addition, which subsequently redissolved upon completion. H_3PO_4 (4 M, 42 mL) was then added dropwise with continuous stirring, affording a clear yellow solution that was heated at 110 °C for 24 h. After the pale-yellow solution was cooled to room temperature, KCl (25 g, 0.34 mol) was added with stirring. The resulting yellow precipitate was collected by filtration and air-dried for 2 h.

The pale-yellow solid was dissolved in water (110 mL), and bromine water was added dropwise until the solution colour changed from green to pale green and yellow. The solution was heated to 90 °C for recrystallisation, cooled overnight, and filtered to give a light-green precipitate. The solid was washed with cold water (2 × 5 mL) and dried to collect a white/green crystalline product (14.9 mg, 36.3%).

^{31}P NMR (162 MHz, D_2O):

δ = -13.02

IR (ATR, cm^{-1}): 3565, 2090, 1602, 1085, 956, 907, 730, 515.

5.3.2 Synthesis of $K_{10}[P_2W_{17}O_{61}]$ (P_2W_{17})

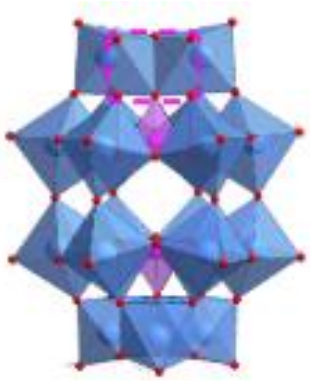

$K_6[P_2W_{18}O_{62}]$ (10.0 g, 2.17 mmol) was dissolved in water (25 mL), followed by the addition of $KHCO_3$ (2.80 g, 33.4 mmol). The mixture was stirred overnight, forming a delicate milky-white suspension. The white precipitate was collected with filtration, washed with water and acetone, and recrystallised using a small amount of hot water (85 ˚C). The solution was then cooled in an ice bath, forming snowy-white crystals, which were isolated by filtration, washed with water and acetone, and dried to yield the final product (7.93 g, 78.3%).[65]

^{31}P NMR (162 MHz, D_2O):

δ = -7.20, -14.38

IR (ATR, cm^{-1}): 3544, 3439, 1078, 1047, 1014, 934, 878, 809, 715, 518.

5.3.3 Synthesis of $K_6[P_2W_{17}O_{57}(PO_3H_5C_6)_2]$

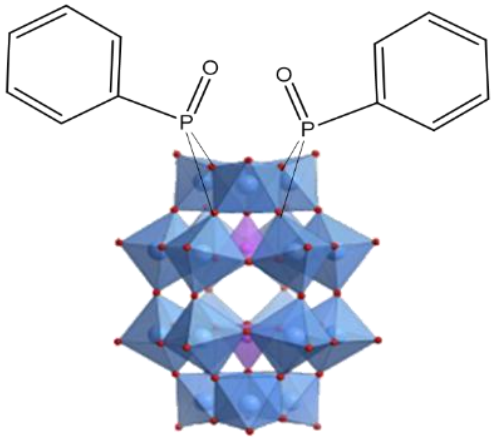

The hybridisation reaction was carried out using a modified procedure based on past research.[80]

$K_{10}[P_2W_{17}O_{61}]$ (250 mg, 0.051 mmol) and phenylphosphonic acid (27.6 mg, 0.175 mmol) were suspended in acetonitrile (12 mL), followed by the addition of HCl (12 M, 40 µL) under stirring. After HCl addition, the white suspension became less cloudy. The mixture was then refluxed at 90 ˚C for 24 h and cooled to room temperature. The white residual solid was removed by centrifugation (8000 rpm, 2 mins), after which diethyl ether (35 mL) was added to induce precipitation of a white suspension. The mixture was centrifuged (8000 rpm, 5 mins) to yield a light green solid. Subsequent centrifugation with EtOH (30 mL) then Et_2O (35 mL) (8000 rpm, 5 mins each) obtained the final product as a light-green powder (164 mg, 69%).

^{1}H NMR (400 MHz, DMSO-d_6):

δ =7.98 (dd, 4H), 7.56 - 7.44 (m, 6H).

^{31}P NMR (162 MHz, DMSO-d_6):

δ = 14.83, -11.34, -12.97.

IR (ATR, cm^{-1}): 3505, 1610, 1463, 1086, 953, 906, 725, 568, 527.

5.3.4 Synthesis of $K_6[P_2W_{17}O_{57}(PO_5H_5C_7)_2]$

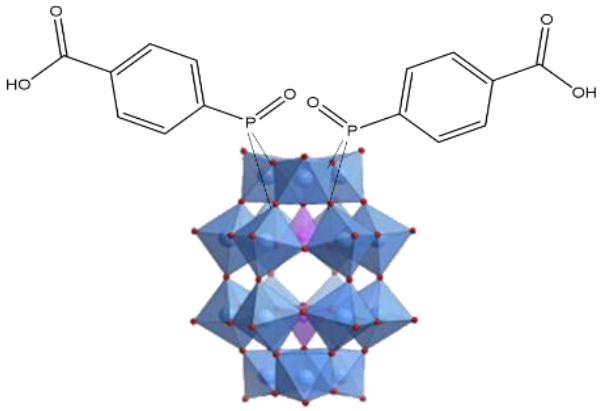

$K_{10}[P_2W_{17}O_{61}]$ (250 mg, 0.051 mmol) and 4-carboxyphenyl phosphonic acid (35.2 mg, 0.175 mmol) were suspended in acetonitrile (12 mL), followed by the addition of HCl (12 M, 40 µL) under stirring. After HCl addition, the white suspension became less cloudy. The mixture was then refluxed at 90 ˚C for 24 h and cooled in an ice bath. The white residual solid was removed by centrifugation (8000 rpm, 2 mins), after which solution was divided into two centrifuge tubes. Diethyl ether (40 mL) was added to each tube to induce precipitation of a white suspension. The mixture was centrifuged (8000 rpm, 5 mins) to form a light green solid. Subsequent

centrifugation with EtOH (10 mL) then Et_2O (40 mL) (8000 rpm, 5 mins each) gave the final product as a light blue powder (130 mg, 51%).

^{1}H NMR (400 MHz, DMSO-d_6):

δ =13.17 (s, 2H), 8.09 (dd, *J*= 13.5, 8.0 Hz, 4H), 8.01(dd, *J*= 8.3, 3.9 Hz, 4H).

^{31}P NMR (162 MHz, DMSO-d_6):

δ = 13.28, -11.35, -12.90.

IR (ATR, cm^{-1}): 3585, 3438, 2997, 1701, 1558, 1097, 953, 914, 862, 796, 584, 541, 531.

5.3.5 Synthesis of $K_6[P_2W_{17}O_{57}(PO_5H_9C_{13})_2]$

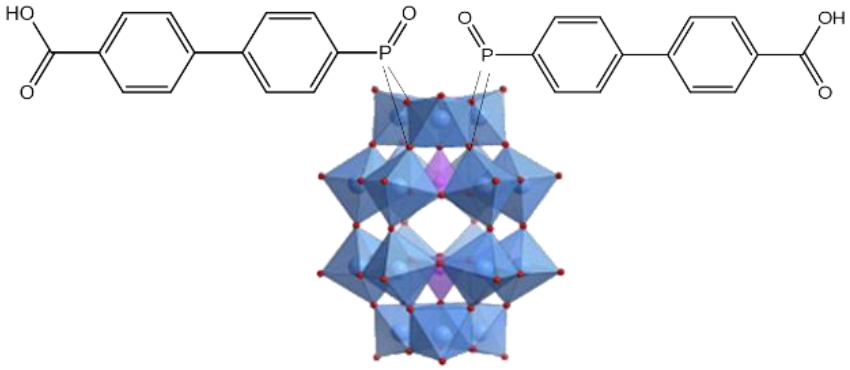

$K_{10}[P_2W_{17}O_{61}]$ (250 mg, 0.051 mmol) and 4-phosphonato-4'-biphenylcarboxylic acid (48.4 mg, 0.174 mmol) were suspended in acetonitrile (12 mL), followed by the addition of HCl (12 M, 40 µL) under stirring. After HCl addition, the white suspension became less cloudy. The mixture was then refluxed at 90 ˚C for 24 h and cooled in an ice bath. The white residual solid was removed by centrifugation (8000 rpm, 2 mins), after which solution was divided into two centrifuge tubes. Diethyl ether (40 mL) was added to each tube to induce precipitation of a white suspension. The mixture was centrifuged (8000 rpm, 5 mins) to form an orange solid. Subsequent centrifugation with EtOH (10 mL) then Et_2O (40 mL) (8000 rpm, 5 mins each) gave the final product as an orange powder (199 mg, 76%).

^{1}H NMR (400 MHz, DMSO-d_6):

δ =12.96 (s, 2H), 8.16 - 8.04 (m, 8H), 7.94 – 7.86 (m, 8H).

^{31}P NMR (162 MHz, DMSO-d_6):

δ = 14.57, -11.31, -12.93.

IR (ATR, cm^{-1}): 2376, 2090, 1703, 1605, 1391, 1086. 953, 907, 721, 588, 528, 474.

5.4 Synthesis of $K_6[P_2W_{17}O_{57}(PO_3H_5C_6)_2]$ derivative cluster

A post-functionalisation hybrid POM cluster was synthesised following a reported method.[74]

$K_6[P_2W_{17}O_{57}(PO_3H_5C_6)_2]$ (139 mg, 0.030 mmol) and $Zn(OAc)_2$ (55.3 mg, 0.301 mmol) were dissolved in an acetonitrile: water (6:1 (v/v)) solution. After filtration, the filtrate was evaporated at room temperature for 1 week, yielding a white powder (88.4 mg, 33%).

^{31}P NMR (162 MHz, DMSO-d_6):

δ = -9.18, -13.47, -14.25

5.5 Attempt Synthesis of POM-based MOF

5.5.1 Synthesis of $K_6[P_2W_{17}O_{57}(PO_5H_5C_7)_2]$ derivative MOF

$K_6[P_2W_{17}O_{57}(PO_5H_5C_7)_2]$ (50 mg, 0.011 mmol) was dissolved in acetonitrile (1 mL), after which triethylamine (4.6 µL) was added and colour was changed from blue to green blue. Zinc acetate anhydrous (5.2 mg, 0.028 mmol) was dissolved in the mixture of MeCN (1 mL) and DMF (0.2 mL). Two solutions were combined and stirred for 1h, then were left over in a fume hood for 3 days to allow slow evaporation. Diethyl ether was added into the remaining of solution, sonicated for 10 min, and the ether was poured out. Acetonitrile with a small amount of ether was added into the vial, followed by sonication for 5 min. The solvent was removed, and the resulting powder was dried under vacuum. The final product was collected by scraping it from the bottom of the vial (41.3 mg).

^{1}H NMR (400 MHz, DMSO-d_6):

δ = 8.79 (s), 8.37 (s), 8.12-8.03 (m), 7.96 (s)

^{13}C NMR (101 MHz, DMSO-d_6):

δ = 162.78

^{31}P NMR (162 MHz, DMSO-d_6):

δ = 10.38, 0.26, -3.08, -11.30, -13.04

5.5.2 Synthesis of $K_6[P_2W_{17}O_{57}(PO_5H_9C_{13})_2]$ derivative MOF

Method A: $K_6[P_2W_{17}O_{57}(PO_5H_9C_{13})_2]$ (53.7 mg, 0.011 mmol) was dissolved in MeCN (2 mL), after which triethylamine (4.6 µL) was added into the yellow solution, forming a brown gel-like material in the vial. Acetic acid (2.5 µL, 0.028 mmol) was added to partially redissolve the gel. Zinc acetate anhydrous (5.2 mg, 0.028 mmol) was dissolved in the mixture of MeCN (0.5 mL) and DMF (0.2 mL). Two solutions were combined and stirred for 1h, then were left over in a fume hood for 3 days to allow slow evaporation. Diethyl ether was added into the remaining of solution, sonicated for 10 min, and the ether was poured out. Acetonitrile with a small amount of ether were added into the vial, followed by sonication for 5 min. The solvent was removed, and the resulting powder was dried under vacuum. The final product was collected by scraping it from the bottom of the vial (18.4 mg).

^{1}H NMR (400 MHz, DMSO-d_6):

δ = 9.95

^{31}P NMR (162 MHz, DMSO-d_6):

δ = 10.80, -11.28, -13.05

Method B: $K_6[P_2W_{17}O_{57}(PO_5H_9C_{13})_2]$ (53.7 mg, 0.011 mmol) was dissolved in MeCN (2.5 mL), after which triethylamine (1.2 µL) was added into the yellow solution. Unlike Method A, no brown gel was formed in the vial. Zinc acetate anhydrous (5.2 mg, 0.028 mmol) was dissolved in the mixture of MeCN (0.5 mL) and DMF (0.2 mL). Two solutions were combined and stirred for 1h, then were left over in a fume hood for 3 days to allow slow evaporation. Diethyl ether was added into the remaining of solution, sonicated for 10 min, and ether was poured out. Acetonitrile with a small amount of ether were added into the vial, followed by sonication for 5 min. The solvent was removed, and the resulting powder was dried under vacuum. The final product was collected by scraping it from the bottom of the vial (42.5 mg).

^{13}C NMR (101 MHz, DMSO-d_6):

δ = 162.82

^{31}P NMR (162 MHz, DMSO-d_6):

δ = 10.65, -11.27, -13.04

5.6 Synthesis of MOF-5

MOF-5 was synthesised following the method reported by Tranchemontagne, Hunt and Yaghi.[75]

Terephthalic acid (254 mg, 1.53 mmol) and triethylamine (425 µL) were dissolved in dimethylformamide (DMF, 20 mL). Zinc acetate dihydrate (850 mg, 3.87 mmol) was dissolved in DMF (25 mL), and the zinc solution was then injected into the organic solution and stirred for 15 min. A white precipitate formed, and the mixture was stirred overnight. The resulting suspension was centrifuged to collect the MOF-5 powder, which was subsequently immersed in DMF (12.5 mL) for 6 h. After centrifugation, the white precipitate was transferred into chloroform (17.5 mL), and the solvent was replaced after 2, 5, and 7 days. The solvent was removed under vacuum to yield a white powder (0.326 g, 83%).

^{1}H NMR (400 MHz, DMSO-d_6):

δ = 9.86

LIST OF REFERENCES

1. A. Dolbecq, E. Dumas, C. R. Mayer, P. Mialane, *Chem. Rev.*, 2010, **110 (10)**, 6009-6048. DOI: 10.1021/cr1000578.
2. D. L. Long, R. Tsunashima, L. Cronin, *Angew. Chem. Int. Ed.,* 2010, **49 (10)**, 1736–1758. DOI: 10.1002/anie.200902483.
3. J. M. Cameron, G. Guillemot, T. Galambos, S. S. Amin, E. Hampson, K. M. Haidaraly, G. N. Newton, G. Izzet, *Chem. Soc. Rev.*, 2022, **51 (1)**, 293–328. DOI: 10.1039/D1CS00832C.
4. T. He, J. Yao, *Prog. Mater*. Sci., 2006, **51(6)**, 810-879. DOI: 10.1016/j.pmatsci.2005.12.00.
5. P. Le Magueres, L. Ouahab, S. Golhen, D. Grandjean, O. Pena, J.-C. Jegaden, C. J. Gomez-Garcia, P. Delhaes, *Inorg. Chem.,* 1994, ***33* (23)**, 5180– 5187. DOI: 10.1021/ic00101a008.
6. N. Mizuno, K. Yamaguchi, K. Kamata, *Coord. Chem. Rev.,* 2005, **249**, 1944-1956. DOI: 10.1016/j.ccr.2004.11.019.
7. S.-S. Wang, G.-Y. Yang, *Chem. Rev.,* 2015, **115 (11)**, 4893–4962. DOI: 10.1021/cr500390v.
8. J. T. Rhule, C. L. Hill, D. A. Judd, R. F. Schinazi, *Chem. Rev.,* 1998, **98 (1)**, 327–358. DOI: 10.1021/cr960396q.
9. U. Kortz, A. Müller, J. van Slageren, J. Schnack, N. S. Dalal, M. Dressel, *Coord. Chem. Rev.,* 2009, **253 (19-20)**, 2315-2327. DOI: 10.1016/j.ccr.2009.01.014.
10. S. Omwoma, W. Chen, R. Tsunashima, Y.-F. Song, *Coordination Chemistry Reviews*. 2014, **258**, 58-71. DOI: 10.1016/j.ccr.2013.08.039.
11. Y.-F. Song, R. Tsunashima, *Chem. Soc. Rev.,* 2012, **41 (22)**, 7384-7402. DOI: 10.1039/C2CS35143A.
12. D.-L. Long, E. Burkholder, L. Cronin, *Chem. Soc. Rev.,* 2007, **36**, 105-121. DOI: 10.1039/B502666K.
13. C. L. Hill, *Chem. Rev.,* 1998, **98**, 1–2. DOI: 10.1021/cr960395y.
14. M. T. Pope, A. Müller, *Angew. Chem. Int. Ed., 1991,* **30 (1)**, 34–48. DOI: 10.1002/anie.199100341.
15. S. Roy, V. Vemuri, S. Maiti, K. S. Manoj, U. Subbarao, S. C. Peter, *Inorg. Chem.*, 2018, ***57***, 12078– 12092. DOI: 10.1021/acs.inorgchem.8b01631
16. A. Müller, E. Krickemeyer, H. Bögge, M. Schimidtmann, F. Peters, *Angew. Chem. Int. Ed.,* 1998, **37**, 3359–3363. DOI: 10.1002/(SICI)1521-3773(19981231)37:24%3C3359::AID-ANIE3359%3E3.0.CO;2-J.
17. A. Misra, K. Kozma, C. Streb, M. Nyman, *Angew. Chem. Int. Ed.,* 2020, **59**, 596–612. DOI: 10.1002/anie.201905600.
18. D.-L. Long, R. Tsunashima, L. Cronin, *Angew. Chem. Int. Ed.,* 2010, **49**, 1736–1758. DOI: 10.1002/anie.200902483.
19. A. Müller, P. Gouzerh, *Chem. Soc. Rev.,* 2012, **41**, 7431-7463. DOI: 10.1039/C2CS35169B.
20. A. Müller, P. Gouzerh, *Chem.-Eur. J.,* 2014, **20**, 4862-4873.

DOI: 10.1002/chem.201305010.
21. T.-L. Lai, M. Awada, S. Floquet, C. Roch-Marchal, N. Watfa, J. Marrot, M. Haouas, F. Taulelle, E. Cadot, *Chem.-Eur. J.,* 2015, **21**, 13311-13320. DOI: 10.1002/chem.201406648.
22. V. S. Korenev, A. G. Boulay, M. Haouas, F. Bannani, V. P. Fedin, M. N. Sokolov, E. Terazzi, S. Garai, A. Müller, F. Taulelle, J. Marrot, N. Leclerc, S. Floquet, E. Cadot, *Chem. Eur. J.,* 2014, **20**, 3097-3105. DOI: 10.1002/chem.201303719.
23. Y. Gao, M. Choudhari, G. K. Such, C. Ritchie, *Chem Sci*., 2022, **13 (9)**, 2510-2527. DOI: 10.1039/D1SC05879G.
24. A. F. Wells, *The London, Edinburgh, and Dublin Philosophical Magazine and Journal of Science*, 1940, ***30* (199)**, 103–134. DOI: 10.1080/14786444008520702.
25. B. Dawson, *Acta Cryst*., 1953, **6 (2)**, 113–126. DOI: 10.1107/S0365110X53000466.
26. S. Vanhaecht, G. Absillis, T. N. Parac-Vogt, *Dalton Trans.,* 2012, **41**, 10028-10034. DOI: 10.1039/C2DT30588G.
27. J. Guo, D. Zhang, L. Chen, Y. Song, D. Zhu, Y. Xu, *Dalton Trans.*, 2013, **42**, 8454-8459. DOI: 10.1039/C3DT50155H.
28. R. Contant, R. Thouvenot, *Inorg. Chim. Acta*., 1993, **212 (1-2)**, 41-50. DOI: 10.1016/S0020-1693(00)92306-5.
29. A. Bijelic, M. Aureliano, A. Rompel, *Chem. Commun*., 2018, **54**, 1153–1169. DOI: 10.1039/C7CC07549A.
30. A. Bijelic, M. Aureliano, A. Rompel, *Angew. Chem. Int. Ed.,* 2019, ***58***, 2980–2999. DOI: 10.1002/anie.201803868.
31. M. Aureliano, *BioChem*., 2022, ***2***, 8-26. DOI: 10.3390/biochem2010002.
32. H. N. Miras, L. Vilà-Nadal, L. Cronin, *Chem. Soc. Rev*., 2014, **43**, 5679-5699. DOI: 10.1039/C4CS00097H.
33. A. V. Anyushin, A. Kondinski, T. N. Parac-Vogt, *Chem. Soc. Rev*., 2020, **49**, 382-432. DOI: 10.1039/C8CS00854J.
34. A. Proust, R. Thouvenot, P. Gouzerh, *Chem. Commun.*, 2008, **16**, 1837-1852. DOI: 10.1039/B715502F.
35. S.-S. Wang, G.-Y. Yang, *Chem. Rev.,* 2015, **115**, 4893–4962. DOI: 10.1021/cr500390v.
36. L. Vilà-Nadal, L. Cronin, *Nat. Rev. Mater.,* 2017, **2**, 17054. DOI: 10.1038/natrevmats.2017.54.
37. A. Proust, B. Matt, R. Villanneau, G. Guillemot, P. Gouzerh, G. Izzet, *Chem. Soc. Rev.,* 2012, **41**, 7605–7622. DOI: 10.1039/C2CS35119F.
38. K. Suzuki, N. Mizuno, K. Yamaguchi, *ACS Catal*., 2018, **8**, 10809–10825. DOI: 10.1021/acscatal.8b03498.
39. G. Kickelbick, *Hybrid Materials: Synthesis, Characterization, and Applications*, Wiley-VCH, Germany, 2007, 1–48. DOI: 10.1002/9783527610495.ch1.
40. S. Berardi, M. Carraro, A. Sartorel, G. Modugno, M. Bonchio, *Israel Journal of Chemistry*, 2011, **51**, 259-274.

DOI: 10.1002/ijch.201100018.
41. A. J. Kibler, V. S. Souza, J. A. Fernandes, W. Lewis, S. P. Argent, J. Dupont, G. N. Newton, *Front. Chem.,* 2021, **8**, 612535. DOI: 10.3389/fchem.2020.612535.
42. B. Kowalewski, J. Poppe, U. Demmer, E. Warkentin, T. Dierks, U. Ermler, K. Schneider, *J. Am. Chem. Soc.,* 2012, **134**, 9768-9774. DOI: 10.1021/ja303084n.
43. O. Linnenberg, A. Kondinski, C. Stöcker, K. Y. Monakhov, *Dalton Trans.,* 2017, **46**, 15636-15640. DOI: 10.1039/C7DT03376A.
44. M. J. Monteiro, *J. Polym. Sci. Part A: Polym. Chem.,* 2005, **43 (15)**, 3189–3204. DOI: 10.1002/pola.20845.
45. O. M. Yaghi, H. Li, *J. Am. Chem. Soc.,* 1995, ***117***, 10401-10402. DOI: 10.1021/ja00146a033.
46. X. Zhao, Y. Wang, D.-S. Li, X. Bu, P. Feng, *Adv. Mater.,* 2018, **30 (37)**, 1705189. DOI: 10.1002/adma.201705189.
47. B. Maranescu, A. Visa, *Int. J. Mol. Sci.,* 2022, ***23***, 4458. DOI: 10.3390/ijms23084458.
48. L. Zhu, X.-Q. Liu, H.-L. Jiang, L.-B. Sun, *Chem. Rev.,* 2017, **117**, 8129-8176. DOI: 10.1021/acs.chemrev.7b00091.
49. Y.-J. Cui, J. Zhang, H.-J He, G.-D. Qian, *Chem. Soc. Rev.,* 2018, **47**, 5740-5785. DOI: 10.1039/C7CS00879A.
50. Y. Cui, B. Li, H. He, W. Zhou, B. Chen, G. Qian, *Acc. Chem. Res.,* 2016, ***49***, 483-493. DOI: 10.1021/acs.accounts.5b00530.
51. T. Rodenas, I. Luz, G. Prieto, B. Seoane, H. Miro, A. Corma, F. Kapteijn, F. X. Llabrés i Xamena, J. Gascon, *Nat. Mater.,* 2015, **14**, 48–55. DOI: 10.1038/NMAT4113.
52. H. Al-Kutubi, J. Gascon, E. J. R. Sudhçlter, L. Rassaei, *ChemElectroChem*, 2015, **2**, 462-474. DOI: 10.1002/celc.201402429.
53. M. Klimakow, P. Klobes, A. F. Thünemann, K. Rademann, F. Emmerling, *Chem. Mater.,* 2010, ***22***, 5216– 5221. DOI:10.1021/Cm1012119.
54. D.-Y. Du, J.-S. Qin, S.-L. Li, Z.-M. Su, Y.-Q. Lan, *Chem. Soc. Rev.,* 2014, **43**, 4615-4632. DOI: 10.1039/C3CS60404G.
55. K. Li, Y.-F. Liu, X.-L. Lin, G.-P. Yang, *Inorg. Chem.,* 2022, ***61***, 6934–6942. DOI: 10.1021/acs.inorgchem.2c00287.
56. N. Song, Y. Li, Y. Wang, M. Wang, M. Liu, L. Chen, J. Zhao, *Inorg. Chem. Front.,* 2022, **9**, 4232-4243. DOI: 10.1039/D2QI00816E.
57. B. Nohra, H. El Moll, L. M. Rodriguez Albelo, P. Mialane, J. Marrot, C. Mellot-Draznieks, M. O'Keeffe, R. Ngo Biboum, J. Lemaire, B. Keita, L. Nadjo, A. Dolbecq, *J. Am. Chem. Soc*., 2011, **133 (34)**, 13363–13374. DOI: 10.1021/ja201165c.
58. Z. Xiao, Y. Mei, S. Yuan, H. Mei, B. Xu, Y. Bao, L. Fan, W. Kang, F. Dai, R. Wang, L. Wang, S. Hu, D. Sun, H.-C. Zhou, *ACS Nano*., 2019, **13**, 7024-7030. DOI: 10.1021/acsnano.9b02106.

59. N. I. Gumerova, A. Rompel, *Chem. Soc. Rev.,* 2020, **49**, 7568-7601. DOI: 10.1039/D0CS00392A.
60. I. -M. Mbomekalle, Y. W. Lu, B. Keita, L. Nadjo, *Inorg. Chem. Commun.,* 2004, **7**, 86-90. DOI: 10.1016/j.inoche.2003.10.011.
61. W. J. Randall, M. W. Droege, N. Mizuno, K. Nomiya, T. J. R. Weakley, R. G. Finke, N. Isern, J. Salta, J. Zubieta, *Inorg. Synth.*, 1997, **31**, 167-185.
62. W. J. Randall, D. K. Lyon, P. J. Domaille, R. G. Finke, A. M. Khenkin, C. Hill, *Inorg. Synth.*, 1998, **32**, 242-268. DOI: 10.1002/9780470132630.ch40.
63. C. R. Graham, R. G. Finke, *Inorg. Chem*., 2008, **47**, 3679-3686. DOI: 10.1021/ic702295y.
64. R. G. Finke, M. W. Droege, P. J. Domaille, *Inorg. Chem*., 1987, **26 (23)**, 3886-96. DOI: 10.1021/ic00270a014.
65. R. Constant, W. G. Klemperer, O. Yaghi, *Inorg. Synth.*, 1990, **27**, 104-111. DOI:10.1002/9780470132586.ch18.
66. S. E. Ashbrook, M. E. Smith, *Chem. Soc. Rev.,* 2006, **35**, 718-735. DOI: 10.1039/B514051J.
67. Y.-G. Chen, J. Gong, L.-Y. Qu, *Coord. Chem. Rev*., 2004, **248**, 245-260. DOI: 10.1016/j.cct.2003.11.003.
68. A. Kruve, K. Kaupmees, J. Liigand, M. Oss, I. Leito, *J. Mass Spectrom*., 2013, **48 (6)**, 695–702. DOI: 10.1002/jms.3218.
69. Q. Jia, Y. Zhang, J. Cao, *Sci. China Chem.,* 2015, **58 (7)**, 1206–1210. DOI: 10.1007/s11426-015-5355-4.
70. W. Jastrzebski, M. Sitarz, M. Rokita, K. Bulat, *Spectrosc. Acta Pt. A: Mol. Biomol. Spectr.*, 2011, **79 (4)**, 722-727. DOI: 10.1016/j.saa.2010.08.044.
71. C. M. Teague, X. Li, M. E. Biggin, L. Lee, J. Kim, A. A. Gewirth, *J. Phys. Chem. B.,* 2004, **108**, 1974-1985. DOI: 10.1021/jp036533m.
72. M. Pascual-Borràs, X. López, J. M. Poblet, *Phys. Chem. Chem. Phys.,* 2015, **17 (14)**, 8723–8731. DOI: 10.1039/C4CP05016A.
73. T. Kusukawa, R. Mura, Y. Ohtagaki, M. Ooe, *Tetrahedron*, 2020, **76**, 131065. DOI: 10.1016/j.tet.2020.131065.
74. J. M. Cameron, S. Fujimoto, R.-J. Wei, G. N. Newton, H. Oshio, *Dalton Trans*., 2018, **47**, 10590-10594. DOI: 10.1039/C8DT01253A.
75. D. J. Tranchemontagne, J. R. Hunt, O. M. Yaghi, *Tetrahedron*, 2008, **64 (36)**, 8553-8557. DOI: 10.1016/j.tet.2008.06.036.
76. C. Rocchiccioli-Deltcheff, R. Thouvenot, *Spectrosc. Lett.,* 1979, **12**, 127–138. DOI: 10.1080/00387017908069138.
77. G. B. McGarvey, J. B. Moffat, *J. Mol. Catal.,* 1991, **69**, 137–155. DOI: 10.1016/0304-5102(91)80110-O.
78. S. Xiang, M. Li, Z. Xia, C. Fang, W. Yang, W. Deng, Z. Tan, *Org. Biomol. Chem.,* 2024, **22**, 1794-1799. DOI: 10.1039/D3OB01987J.
79. C. Heering, B. Francis, B. Nateghi, G. Makhloufi, S. Lüdeke, C. Janiak, *CrystEngComm*., 2016, **18**, 5209-5223. DOI: 10.1039/C6CE00587J.

80. J. M. Cameron, S. Fujimoto, K. Kastner, R.-J. Wei, D. Robinson, V. Sans, G. N. Newton, H. H. Oshio, *Chemistry Europe*., 2017, **23 (1)**, 47-50. DOI: 10.1002/chem.201605021.